HHS Public Access

Author manuscript

Contrast Media Mol Imaging. Author manuscript; available in PMC 2016 July 01.

Published in final edited form as:

Contrast Media Mol Imaging. 2015 July ; 10(4): 245–265. doi:10.1002/cmmi.1629.

A review of responsive MRI contrast agents: 2005–2014

Dina V. Hingorani[1], **Adam S. Bernstein**[2], and **Mark D. Pagel**[1,2,3,4]

[1]Department of Chemistry and Biochemistry, University of Arizona

[2]Department of Biomedical Engineering, University of Arizona

[3]Department of Medical Imaging, University of Arizona

[4]University of Arizona Cancer Center, University of Arizona

Abstract

This review focuses on MRI contrast agents that are responsive to a change in a physiological biomarker. The response mechanisms are dependent on six physicochemical characteristics, including the accessibility of water to the agent, tumbling time, proton exchange rate, electron spin state, MR frequency, or superparamagnetism of the agent. These characteristics can be affected by changes in concentrations or activities of enzymes, proteins, nucleic acids, metabolites, or metal ions, or changes in redox state, pH, temperature, or light. A total of 117 examples are presented, including examples that employ nuclei other than ^{1}H, which attests to the creativity of multidisciplinary research efforts to develop responsive MRI contrast agents.

Keywords

MRI contrast agents; responsive agents; T_1 agents; T_2* agents; CEST agents; MRS agents; hyperpolarized agents

1. Introduction

Magnetic resonance imaging (MRI) has developed from a confounding problem with spatial magnetic field inhomogeneity during NMR spectroscopy, to a valuable diagnostic technique during this century (1). As evidence for the popularity of clinical MRI diagnoses, MRI exams in the USA have increased approximately 10% per year from 1996 to 2010, with about 28.2 million clinical MRI scans performed in 2010 (2,3). The development of exogenous MRI contrast agents has paralleled the engineering of MRI instrumentation, with the first *in vivo* MRI studies of contrast agents with Fe(III), Mn(II), nitroxide radicals, and Gd(III) reported in 1981–1984 (4–9). The use of exogenous MRI contrast agents for enhancing clinical diagnoses has also grown in popularity, as roughly 35% of all clinical MRI scans in the USA in 2010 employed an exogenous MRI contrast agent (10).

Exogenous MRI contrast agents were initially developed to enhance the image contrast of anatomical features (9). For example, MR neuroimaging with exogenous contrast agents

Corresponding author: Mark “Marty” Pagel, University of Arizona Cancer Center, 1515 N. Campbell Ave., Tucson, AZ 85724-5024, Tel: (520)-404-7049, FAX: (520)-626-0395, mpagel@u.arizona.edu.

routinely depicts disruption of the blood-brain barrier and the morphological details of cerebral lesions (11). MRI contrast agents can also be used to localize the ischemic, acutely infarcted, and peri-infarcted myocardium in occlusive and reperfused myocardial infarctions (12). MRI contrast agents for anatomical diagnoses are typically designed to exploit differential uptake of the MRI contrast agent in pathological and normal tissues, and therefore primarily behave as “static tracer agents” that do not change their physicochemical properties.

The availability of clinical MRI scanners in the 1980s and early 1990s provided the opportunity for clinicians to develop and employ MRI contrast agents for studying tissue function (13). For example, MRI contrast agents are routinely administered to patients and animal models to track vascular flow for large arteries and veins using MRI angiography (14). These exogenous agents can also track vascular perfusion and permeability in capillary networks using Dynamic Contrast Enhancement MRI methods (15). These contrast agents primarily behave as tracer agents that change in concentration in various organs, but do not experience a deliberate change in their physicochemical properties during the MRI study.

MRI contrast agents have also been developed for molecular imaging (16). Although MRI does not have sufficient sensitivity to image single molecules, MRI can detect molecular compositions or environmental characteristics of the tissue. MRI contrast agents can detect differences or changes in molecular compositions and therefore have a prominent role in the development of MRI for molecular imaging. Responsive agents dynamically change one or more of their physicochemical properties when interacting with their intended molecular biomarker, and therefore differ from static tracer agents. A multidisciplinary research approach is often required to develop and apply responsive MRI contrast agents to biological or biomedical studies, including an understanding of chemistry and biochemistry, molecular and cell biology, physiology, radiology, and biomedical engineering of imaging methods.

We have previously reviewed 54 responsive MRI contrast agents reported during or before 2007, with an emphasis on classifying agents based on physicochemical characteristics, and how these physicochemical characteristics can be employed to detect a response from each type of biomarker (17). This current review classifies an additional 117 responsive MRI contrast agents reported since 2005. Furthermore, this review includes agents that employ nuclei other than ^{1}H. As with our previous review, an emphasis is placed on the multidisciplinary approach that was required for the development of these recently reported MRI contrast agents, and that will be required for further development of these responsive agents.

To facilitate the classifications of these responsive MRI contrast agents, we have limited the scope of our review to agents that experience a change in one or more of their physicochemical characteristics when interacting with a physiological biomarker. This scope excludes some types of MRI contrast agents for molecular imaging. For example, MRI contrast agents that non-covalently bind to cell receptors or covalently bind and inhibit enzymes are primarily used to detect differences in pharmacokinetic retention in pathological tissues relative to surrounding normal tissues (18,19). This difference in

pharmacokinetics does not necessarily require a change in the agent's physicochemical characteristics. Similarly, MRI contrast agents that are internalized into cells via reporter gene systems, or are otherwise preferentially retained in specific tissue types, depend on a difference in pharmacokinetics (20,21). Although changes in the agent's physico-chemical characteristics may also occur, these changes in physicochemical characteristics are secondary to the pharmacokinetic retention. These non-responsive MRI contrast agents are described in other outstanding reviews, and are therefore not considered in this review (22,23).

Responsive MRI contrast agents that match our scope have been occasionally described as "smart" MRI contrast agents (24). However, this term is anthropomorphic, and therefore has become less popular for describing a chemical. Responsive MRI contrast agents have also been described as "activatable" agents (25). Yet some MRI contrast agents become de-activated when interacting with their intended biomarker, which is a valid approach especially if a second unresponsive agent can be included as an internal control. For these reasons, the term "responsive MRI contrast agent" is preferred in this review.

2. MRI contrast mechanisms

Unlike most other biomedical imaging modalities, MRI can generate image contrast through a variety of contrast mechanisms. T_1, T_2, and T_2* image contrasts are direct results of the relaxation properties of the nuclei of interest. Chemical Exchange Saturation Transfer (CEST) contrast is generated from the kinetic exchange properties of the agent. The MR chemical shift of the CEST effect and of MR spectroscopy agents are influenced by the electronic shielding of the nucleus of interest. Six physicochemical characteristics can affect these MR contrast mechanisms, providing fundamental mechanisms that can be exploited for molecular imaging. These six characteristics are the agent's tumbling time; electron spin state; distance between two dipoles; superparamagnetism; chemical exchange rate; and chemical shift (Fig. 1).

The T_1 relaxation time constant describes the time after excitation for the magnetization to return to the equilibrium ground state (26). This return to energy equilibrium is accomplished by transferring the excess energy of the magnetic spins of the excited ^{1}H nuclei (protons) to the surrounding lattice, thereby giving the T_1 relaxation time constant the alias 'spin-lattice relaxation time constant'. Because the direction of the net magnetization in the equilibrium ground state lies along the axis of the main magnetic field of the MRI scanner, T_1 relaxation is also known as 'longitudinal relaxation'. The excess energy can be transferred through a dipole-dipole interaction, which is influenced by three physicochemical characteristics: the tumbling times of the two dipoles that exchange energy; the electron spin state of one of the dipoles; and the distance between the two dipoles. Therefore, responsive T_1 contrast agents can undergo a change in size to change tumbling time, which can change T_1 relaxation time constant of the system. Responsive T_1 contrast agents can also experience a change in their accessibility to water, by changing the number of water molecules that are associated with the agent, or by changing the average distance between the agent and the water molecules.

MRI contrast agents that cause a decrease in the T_1 relaxation time constant result in a brightening of the MR image, due to the methodology of a T_1-weighted MRI acquisition protocol, and are therefore often known as 'positive-contrast agents' (Fig. 2) (27). T_1-weighted MR images can be acquired in rapid succession to track the dynamics of the agent, which can facilitate the detection and analysis of responsive MRI contrast agents. T_1 MRI contrast agents typically require a minimum concentration of approximately 10 to 500 μM for detection, depending on the quality of the MRI scanner and the biomedical imaging application (28).

T_2 relaxation is associated with the dephasing process of coherent, detectable net magnetization in a plane that is transverse to the direction of the main field of the MRI spectrometer magnet, and therefore the T_2 relaxation time constant is also known as 'transverse relaxation time constant' (26). This dephasing occurs through a dipole-dipole interaction between two protons, thereby earning the name 'spin-spin relaxation'. T_2* relaxation is a dephasing of the detectable net magnetization caused by local magnetic field inhomogeneities. For example, a superparamagnetic iron oxide nanoparticle (SPION) can create a local magnetic field, which strongly interacts with the protons of nearby water molecules. This interaction weakens as a function of distance. T_2* relaxation is primarily influenced by two physicochemical characteristics: the tumbling time of the agent and the magnitude of the agent's superparamagnetism that causes the local magnetic field inhomogeneities. Therefore, responsive T_2* contrast agents can change in size to change tumbling time or water accessibility, or can change the aggregation state of the SPION or other paramagnetic particles to change the superparamagnetism.

Using a T_2* weighted imaging protocol, T_2* contrast agents cause a darkening of the image and are typically considered to be 'negative-contrast agents' (27), although more complicated methods can detect positive image contrast from T_2* MRI contrast agents (29). Dynamic Susceptibility Contrast MRI can be used to monitor the pharmacokinetic of T_2* agents *in vivo* (Fig. 3; 30). In addition, T_2* relaxation time constants are shorter than T_1 relaxation time constants, which may reduce the dynamic range of detection sensitivity for T_2* agents relative to T_1 agents. T_2* agents can be detected at concentrations approaching 1 μM, which is a substantial advantage relative to T_1 agents when detecting the response of a MRI contrast agent to a molecular biomarker (31).

CEST generates MR image contrast through a mechanism that is substantially different than T_1- and T_2*-relaxation. CEST is generated by saturating the coherent net magnetization of equivalent protons on a CEST agent (or a water molecule that is transiently bound to the agent), and then allowing for the transfer of this saturation from the agent to surrounding bulk water through the natural chemical exchange of protons between the agent and water (32). This process results in a decrease in the bulk water MR signal, leading to a darkening of the MR image. The labile protons of the CEST agent have a different chemical shift than that of bulk water. Therefore, acquiring a series of MR images with different saturation frequencies can be used to create a CEST spectrum that shows the decrease in water signal when the chemical shift of the labile protons are saturated, relative to the saturation at other chemical shifts (Fig. 4). A CEST agent's chemical exchange rate and chemical shift are the

two physicochemical characteristics that can be exploited to create responsive CEST MRI contrast agents.

Exogenous diamagnetic CEST (DIACEST) agents are metal-free organic molecules (33). The labile protons of a DIACEST agent typically reside on amide, amine, thiol or hydroxyl chemical groups, which have a range of chemical exchange rates that can be exploited to create responsive MRI contrast agents. The chemical shift difference between the DIACEST agent's exchangeable proton and water is a limited range of approximately 0.8 to 10 ppm. Tracking changes in the chemical shift from a DIACEST agent can be used to track a molecular biomarker, although the limited range of chemical shifts can reduce the practicality of this approach. Perhaps more importantly, this limited chemical shift range can often complicate the saturation of the magnetization of the proton on the agent without also directly saturating some of the magnetization of the water's protons. This complication often requires a minimum concentration of ~5 mM for detecting a DIACEST agent. Yet these agents are typically biocompatible, and have been administered at injection concentrations approaching 1 M, so that tissue concentrations of DIACEST agents can meet the minimum detection threshold.

Paramagnetic CEST (PARACEST) agents comprise a lanthanide ion and an organic chelate, although chelates with metals other than lanthanides have also been used to create PARACEST agents (34–36). PARACEST agents can generate CEST from amide, amine, thiol, hydroxyl or phosphate chemical groups on the agent, or from a water molecule that is non-covalently, transiently bound to the agent. The hyperfine contact shift effect of a metal can cause greater chemical shift differences between the protons on the agent and water. This facilitates the tracking of changes in the chemical shift from a PARACEST agent to track a molecular biomarker. The greater chemical shift differences can also create better specificity for saturating the proton on the PARACEST agent without also directly saturating some of the water's protons. In addition, a CEST agent must have a chemical shift relative to water that is larger than the agent's chemical exchange rate (to avoid a phenomenon known as MR coalescence). Therefore, a PARACEST agent with a greater chemical shift can also have a greater chemical exchange rate, and a greater rate can generate a CEST effect with a greater amplitude. The improved sensitivity can lower the minimum detection limit to ~1 mM metal ion concentration. However, potential toxicity limits the administration of PARACEST agents to levels that are near this minimum detection limit, which limits the detectability of PARACEST agents during *in vivo* studies.

Magnetic resonance spectroscopy and spectroscopic imaging (MRS/I) can also be used to track the chemical shift of a responsive contrast agent (Fig. 5; 37). ^{1}H MRS/I has been used to assess exogenous contrast agents, although detecting the small ^{1}H signal of the agent relative to large ^{1}H signal of water in the tissue can be challenging (38–40). Therefore, responsive contrast agents for MRS/I studies have exploited the detection of ^{11}B, ^{19}F, and ^{31}P from the agent because the endogenous background ^{11}B, ^{19}F, or ^{31}P signal is either negligible or does not overwhelm or overlap with the signal from the agent (41–43). These agents show a change in chemical shift when interacting with a biomarker. The detection sensitivity can range from ~1 to 100 mM on a per-atom basis, depending on the quality of the heteronuclear detector system of the MRI scanner.

Hyperpolarization is a promising method for improving the detection sensitivity of some nuclei during MRS/I studies, especially for ^{13}C, ^{89}Y, and ^{129}Xe (Fig. 6; 44–46). Hyperpolarization of ^{13}C and ^{89}Y is often accomplished by enhancing the spin polarization of the electrons by cooling to low temperature in a magnetic field or through chemically induced processes, and then transferring this spin polarization from electrons to nuclei through a process known as dynamic nuclear polarization. For comparison, ^{129}Xe is commonly hyperpolarized through spin exchange optical pumping with rubidium. Due to the signal enhancement, the minimum concentration needed to detect a hyperpolarized agent can be reduced as much as 10,000-fold compared to standard MRS/I contrast agents. The limited lifetime of hyperpolarization is a potential limitation, particularly for ^{13}C studies. To address this pitfall, permanently-labeled ^{13}C- and ^{31}P-labeled molecules have also been used to follow metabolism, and ^{2}H-labeled metabolites have used to follow rate limiting steps of enzyme catalysis. Technical hurdles, the limited variety of agents, and the additional expense of hyperpolarized MRS/I have inhibited the use of this method, although extensive efforts are being invested to overcome these challenges.

3. Responsive MRI contrast agents: Sensitivity and Specificity

Based on the detection thresholds listed above, at least 1 μM of exogenous contrast agent is required for detection with MRI, and some contrast mechanisms require more than 10 mM for adequate detection (28,31,32,34). This indicates that MRI is a relatively insensitive biomedical imaging modality. This limited sensitivity often requires a high concentration of the biomarker to be detected with responsive MRI contrast agents. As an example, the *in vivo* concentrations of metal ions during physiological processes can reach the concentration threshold for direct detection with a responsive MRI contrast agent. In addition to detecting the biomarker's concentration, consideration should be given to detecting a change in the biomarker's concentration during the physiological process. For example, the *in vivo* concentrations of metal ions may be sufficiently high to detect, but a small change in concentration required for neural activity, cell signaling, or other physiological events may be too low to be accurately determined, rendering the MRI methodology to be ineffective for interrogating the physiological process.

Some responsive MRI contrast agents have physicochemical characteristics that return to their original states when the MRI contrast agent no longer interacts with a molecular biomarker. These agents are known as reversible responsive MRI contrast agents, and have merits for monitoring rapidly changing physiological conditions (47). However, the detection sensitivities of these agents are inherently limited by the concentration of the biomarker, so that the biomarker concentrations must often be high for practical detection of the reversible responsive MRI contrast agent. As an example, a responsive MRI contrast agent that reversibly binds to a metal ion is well suited to monitoring rapid changes of high concentrations of ion flux.

Alternatively, some responsive MRI contrast agents have physicochemical characteristics that do not return to their original states when the MRI contrast agent no longer interacts with a molecular biomarker. These agents are known as irreversible responsive MRI contrast agents (48). Their detection sensitivities are limited by the accumulation of agent that can be

irreversibly altered before the MRI detection. By optimizing the timing of detection, a much greater concentration of irreversibly altered agent may be present relative to the biomarker, which can amplify the detection sensitivity. This optimal timing of the detection often obviates the need to monitor rapidly changing physiological conditions. As an example, an irreversible responsive MRI contrast agent is well suited to detect the presence of the enzyme, because a low concentration of enzyme can rapidly affect a high concentration of agent.

In addition to sensitivity, the specificity of detecting the intended biomarker is a substantial challenge when using responsive MRI contrast agents during practical biomedical applications. In particular, the T_1-weighted or T_2*-weighted MR signal amplitude, the amplitude of a CEST MR measurement, and the amplitude of a MR spectral peak are each dependent on the concentration of the agent. Because pharmacokinetic wash-in and wash-out within *in vivo* tissues is spatially and temporally variable, the concentration of a responsive MRI contrast agent should be taken into consideration to ensure that the contrast agent's response is specific for the intended biomarker. For example, a MRI contrast agent has been labeled with a PET agent to improve the measurement of pH (49). The PET agent was used to track the dynamically varying concentration of the agent in tissues, and this concentration information was used to convert the concentration-dependent T_1-weighted MR signal to a concentration-independent T_1 relaxivity measurement. Similar attempts have used T_2* relaxation to track the concentration of a T_1-responsive MRI contrast agent, although the strong correlations between T_1 and T_2* relaxation mechanisms cause the analysis of these imaging results to be very challenging (50).

As an alternative approach, the chemical shift of a MR spectroscopy agent or a CEST agent is concentration-independent, and therefore these agents that change chemical shift have excellent specificity for detecting the intended biomarker. Furthermore, the measurement of chemical shifts is very precise and accurate, due to decades of technological improvements derived from NMR spectroscopy research studies. In addition, chemical shifts are selectively detectable, providing opportunities to selectively detect an unresponsive "control" agent while also detecting the responsive agent. If the control agent is designed to generate MR signal that is dependent on the same concentration and other environmental conditions as the responsive agent, then the results from the control agent can be used to cancel these effects from the results with the responsive agent, leaving only the results of the specific detection of the intended biomarker. For example, an enzyme-responsive CEST agent and an unresponsive control CEST agent have been co-administered to a mouse model of mammary carcinoma, and the comparison of the CEST effects of these two agents improved the detection of enzyme activity (51).

4. Examples of responsive MRI contrast agents

The chemical structures of the responsive MRI contrast agents described below are available in the Supporting Information.

4.1. Responsive MRI contrast agents that are catalyzed by enzymes

Enzymes are responsible for most of the functions in cellular and molecular biology, and therefore represent a major class of molecular biomarkers. However, many enzymes are initially expressed as zymogens with an inactive form, and are eventually activated when needed by the cell or tissue. Therefore, the detection of the presence of an enzyme may inadvertently detect an inactive enzyme that is not correlated with the progression or treatment of disease states. To avoid this pitfall, contrast agents can be designed to detect the activity level of the enzyme rather than the presence of the enzyme. Responsive MRI contrast agents are useful for assessing enzyme activities in disease states. A low concentration of active enzyme can rapidly create a high concentration of modified contrast agent, which amplifies the sensitivity for detecting the enzyme.

An enzyme can alter the covalent bond structure of a PARACEST agent, resulting in a change in chemical exchange rate of the labile proton of the CEST agent, which causes the CEST effect to appear, disappear, or change in magnitude. For example, a PARACEST agent with a peptide ligand has an amide bond that is cleaved by urokinase Plasminogen Activator (uPA), which converts the amide to an amine, and causes a disappearance of the CEST effect from the amide group of this responsive agent (52). A comparison of this responsive agent with an enzyme-unresponsive “control” agent facilitated the *in vivo* detection of uPA activity (51). A similar PARACEST agent with a different peptide ligand can detect cathepsin-D activity (53). By simply replacing the peptide ligand of such agents, the agent becomes responsive to different enzymes, suggesting that this agent design can act as a platform technology for the detection of many other enzymes. It has recently been shown that the opposite reaction, a formation of an amide bond from an amine group, can also create or change a CEST effect from a responsive agent that detects transglutaminase activity (54). This latter example also showed that enzyme catalysis can also change the chemical shifts of the CEST effect, which can be exploited to detect enzyme activity.

Modular designs of enzyme-responsive PARACEST agents have created platform technologies that may be conveniently modified to detect a variety of enzymes (Fig. 7). For example, a Yb(III) chelate with a β-galactose ligand generates CEST after β-galactosidase cleaves the agent’s ligand, which generates an electron donating group that promotes aromatic delocalization, which further truncates the ligand and creates an amine group that can generate CEST (55). In another example, a Yb(III) chelate with an ester group that caps a trimethyl lock moiety can detect esterase activity through the appearance of CEST after de-esterification triggers an intramolecular lactonization that produces an amine group on the responsive agent (56). These examples demonstrate the advantages of a multidisciplinary research approach that combines the biochemistry of the agent’s enzyme-cleavable trigger, the organic chemistry of the agent’s spontaneous disassembly, and the physical chemistry of the imaging agent.

DIACEST agents have also been developed that detect enzyme activity. For example, cysteine deaminase can covert a cytosine ligand to a uracil moiety on a DIACEST agent, causing a disappearance of CEST from the agent as demonstrated *in vitro* (57). Because cysteine deaminase can convert 5-fluorocytosine into 5-fluorouracil that can act as a

chemotherapeutic agent, this DIACEST agent may be used to track enzyme-based prodrug therapy in tumors. As another example, the peptide $(LRRASLG)_8$ has a reduced CEST effect when Protein Kinase A phosphorylates the serine amino acid residue of this peptide, thereby detecting the kinase activity of this enzyme *in vitro* (58). These examples show that DIACEST agents can also detect both bond cleavage and bond formations that are catalyzed by enzymes.

Enzymes can change the tumbling time of a responsive contrast agent, which can lead to a change in T_1 relaxation time constant. A β-galactopyranose-containing Gd(III) complex undergoes hydrolysis by β-galactosidase, resulting in formation of a reactive phenolate anion (59). This reactive group binds the contrast agent to a protein, slowing the tumbling time of the contrast agent and decreasing T_1 relaxation time constant of the system, as tested *in vitro* and *in vivo*. Similarly, myeloperoxidase can cause a hydroxytriamine ligand of a Gd(III) chelate to form a radical, which can bind the contrast agent to a protein and decrease T_1 relaxation time constant (60). Another Gd(III) chelate has a peptide ligand that is cleaved by legumain, which causes the agent to bind to human serum albumin and decrease the T_1 relxation time constant (61). As another example, Gd-DOTA-tyr-gal is converted to GdDOTA-tyr by β-galactosidase (62,63). The product then undergoes oligomerisation by tyrosinase, creating a large molecular system with a slower tumbling time that decreases the T_1 relaxation time constant of the system. Using the same approach, the peptide of a Gd(III) chelate is cleaved by furin, and a disulfide bond in the remaining peptide ligand is reduced, allowing for dimerization and self-assembly of the agents to form a macrocyclic nanoparticle (64). The slower tumbling time of the nanoparticle causes a decrease in the T_1 relaxation time constant of the system. These results have been validated *in vitro* and *in vivo*, and represent yet another modular design that can be exploited as a platform technology for enzyme detection.

Enzymes can change the accessibility of water for the agent, which can change T_1 relaxation time constant. An interesting example exploits a decrease in solubility when a MMP-7 or MMP-2 enzyme cleaves a PEG-peptide ligand of Gd-DOTA (65,66). The loss of the highly soluble PEG groups causes the remainder of the agent to precipitate from solution, which increases T_1 relaxation time constant that can be detected during *in vivo* studies. The same concept was used to develop a responsive contrast agent that detects lipase activity in cells. Lipase-catalyzed cleavage of the agent's aliphatic ligands allows the agent to become soluble, which decreases the T_1 relaxation time constant of the system, as shown during *in vitro* studies (67) and *in vivo* tests (68). Protamine-linked liposomes that carry a Gd(III) chelate can be disassembled with trypsin, causing greater water accessibility for the agent that creates an decrease in T_1 relaxation time constant (69).

Water accessibility has also been modulated by changing the number of carboxylate groups of the agent. Esterase can create carboxylate groups after cleaving ethyl ester ligands of a Gd(III) chelate, causing displacement of serum anions that allows for more water accessibility to the Gd(III) ion (70). Conversely, glutamic acid decarboxylase activity causes decarboxylation of the glutamine ligands of a Gd(III) chelate, which improves the accessibility of the surrounding water for the Gd(III) ion, resulting in a decrease in T_1 relaxation time constant (71). Tyrosinase can polymerize a Mn(II) chelate, which

destabilizes the chelate and releases the Mn(II) ion, thereby improving accessibility of water for the Mn(II) ion and decreasing T_1 relaxation time constant (72). These examples demonstrate that water accessibility can be decreased or increased to change the responsiveness of the agent, and typically use an irreversible approach to change accessibility via enzyme activity.

Commercially available histological stains have been explored as responsive T_2* agents for detecting enzyme activity. S-Gal, a derivative of β-D-galactopyranoside, was originally developed as a colorimetric agent for measuring β-galactosidase activity *in vitro* and *in vivo* (73,74). On action of β-galactosidase, the generated aglycone chelates Fe^{3+}, forming a superparamagnetic MRI contrast agent that decreases the T_2* relaxation time constant of the system. S-Gal has been used to detect β-galactosidase activity during *in vivo* studies a MCF7-LacZ tumor model. Interestingly, the chelate can shorten the T_1 relaxation time constant before catalysis by β-galactosidase, which provides the opportunity to monitor the delivery of the agent to tissues that have low β-galactosidase activity. Similarly, the T_2* relaxation time constant of the system containing SPION-loaded ferritin can decrease when protein domains incorporated onto the ferritin surface are phosphorylated by protein kinase A, which causes the ferritin to aggregate (75). In three similar examples, the formation of a superparamagnetic MRI contrast agent can be generated when dextranase, MMP-2 or MMP-9 protease cleaves the hydrophilic coating of a SPION, causing the nanoparticles to aggregate and decrease the T_2* relaxation time constant of the system (76–78). Using the same concept, but in the opposite sense, aggregated SPIONs linked via complimentary stands of DNA can be used to detect the activity of the restriction enzyme EcoRV, which cleaves the DNA and irreversibly disaggregates the SPIONs, resulting in an increase in T_2* relaxation time constant of the system (79). A similar example also generated a change in T_2* relaxation following disaggregation of DNA-linked SPIONs during *in vitro* studies, when secreted alkaline phosphatase de-phosphorylates 2′-AMP to create adenosine, which then disrupts a DNA duplex that links the SPIONs (80). Although disaggregation generally increases T_2* relaxation time constant by reducing the superparamagnetism of the system, disaggregation of highly aggregated systems can decrease the T_2* relaxation time constant by improving water accessibility to the system. For example, a sample containing a hydrogel with a very high local concentration of SPIONs has a high T_2* relaxation time constant, and disaggregation of the SPIONs after trypsin digestion decreases the T_2* relaxation time constant (81). Each of these examples exploits an irreversible response for detecting enzyme activity.

Changes in the relaxation rates of ^{19}F have also been exploited to detect enzyme activity. For example, a Gd(III) chelate has been linked to a trifluoromethoxy benzyl group via a caspase-3-cleavable peptide sequence (82). The close proximity of the Gd(III) ion and the trifluoromethoxy group causes a short ^{19}F T_2 relaxation time, rendering ^{19}F MRS/I impractical. Upon proteolysis by caspase-3, the ^{19}F-labeled ligand dissociates from the Gd(III) chelate, and the ^{19}F T_2 relaxation time becomes sufficiently long for practical MRS/I detection. Another contrast agent exploits a similar mechanism by coupling a fluorinated ligand to a Gd(III) chelate with a lactam linker, which creates a T_2 relaxation time that is too short for practical ^{19}F MRS/I detection (83). Cleavage of the linker by β-lactamase releases

the fluorinated ligand, which increases the ^{19}F T_2 relaxation time and allows for the detection of ^{19}F MRS/I signal. Similarly, a Gd(III) chelate has a galactose moiety that can be cleaved by β-galactosidase, which causes aromatic delocalization and subsequent release of a ^{19}F-labeled ligand, eliminating the paramagnetic relaxation enhancement effect, allowing for the detection of ^{19}F MRS/I signal (84). The modular design of this agent may represent a platform technology for enzyme detection. These three examples demonstrate the merits of detecting nuclei other than ^{1}H, because the appearance of a single ^{1}H signal in a crowded ^{1}H MR spectrum of endogenous tissue would be extremely difficult.

Changes in the chemical shifts of ^{19}F and ^{31}P have also been used to detect enzyme activity. For example, fluorinated substrates of β-galactosidase experience a 6–10 ppm change in ^{19}F chemical shift upon cleavage by the enzyme, which can be used to detect β-galactosidase activity *in vitro* and *in vivo* (85). ^{31}P MR spectroscopy has been used to monitor the change in chemical shift as inorganic phosphate is converted to polyphosphate by vacuolar H^+-ATPase (43). A phosphate group experiences a 3 ppm change in ^{31}P chemical shift when the phosphate is transferred from γ position of ATP to phosphocreatine by creatine kinase (86). To detect this change in chemical shift, the magnetic resonance signal of the γ-ATP phosphate was reduced by applying selective radio frequency saturation, which "magnetically labeled" this phosphate group on ATP. When the magnetically labeled phosphate group was transferred from ATP to creatine via enzyme activity, the magnetic resonance signal of the phosphocreatine enzyme product decreased during *in vitro* and *in vivo* studies. This latter example demonstrates the advantages of a multidisciplinary approach that combines the physics of MR saturation experiments and the biochemistry of creatine kinase to detect enzyme activity.

MRS/I of many ^{13}C-hyperpolarized agents have been used to detect enzyme activity by monitoring a change in ^{13}C chemical shift before and after enzyme catalysis. MRS/I of hyperpolarized [1-^{13}C]pyruvate has been associated with the detection of pyruvate dehydrogenase activity, while MRS/I of [2-^{13}C]pyruvate detects the activity of the Krebs cycle (87). In addition, hyperpolarized pyruvate has also been used to detect the activities of alanine transaminase, carbonic anhydrase, mitogen-activated protein kinase, lactate dehydrogenase, and choline kinase α (88–92). Yet MRS/I of hyperpolarized pyruvate and associated hyperpolarized metabolites lactate, alanine, and fumarate, should be considered to be a molecular imaging method that reports on general metabolism rather than the activity of a specific enzyme, because many enzymes are involved in many biochemical pathways that can process these metabolites (93–95). As additional examples, [5-^{13}C]glutamine, 1-keto[1-^{13}C]isocaproate, diethyl[1-^{13}C]succinate, [2-^{13}C]fructose, and 3,5-diflurorbenzoylglutamic acid have been used to detect the activities of glutaminase, branched chain amino acid transaminase, succinate dehydrogenase, hexokinase, and carboxypeptidase G2, respectively (96–100). Yet similar caution is needed to assign the MRS/I of these hyperpolarized agents to only one enzyme activity, because these agents are involved in multiple metabolic pathways with multiple enzymes.

4.2. Responsive MRI contrast agents that detect proteins

MR spectroscopy of hyperpolarized ^{129}Xe has been employed to detect proteins (Fig. 8; 101–103). This noble gas can be chelated by a modified cryptophane cage. When a ligand of the cryptophane non-covalently binds to a target protein, the change in electronic distribution within the agent causes a small change in the chemical shift of ^{129}Xe. The high detection sensitivity of hyperpolarized ^{129}Xe facilitates the detection of concentrations of target protein as low as 10 μM. This approach represents a potential platform technology, although examples of this technology for the detection of proteins with hyperpolarized ^{129}Xe has not yet been realized *in vitro* or *in vivo*.

4.3. Responsive MRI contrast agents that detect nucleic acids

The DNA concentration in cells is typically far below the ~1 μM limit for detection with responsive MRI contrast agents, which severely limits the development and application of responsive MRI contrast agents that detect nucleic acids. However, gene delivery systems can carry a high payload of DNA that can exceed the MRI detection threshold. To be applicable for tracking many types of gene deliveries, a responsive MRI contrast agent should be designed to be nonspecific for a DNA sequence. For example, a polymeric Eu(III) PARACEST agent shows a decrease in CEST when interacting with DNA at 1 mM monomer concentration, due to a change in the chemical exchange rate of a water molecule that is bound to the Eu(III) ion (104). As another example, magnetite spheres with DNA intercalators can bind to DNA duplexes at 0.5 mM base pair concentration (Fig. 9; 105). Although aggregation typically causes an increase in superparamagnetism of the system, the extreme aggregation of magnetite in this example reduced water accessibility and superparamagnetism, causing the T_2* relaxation time constant of the system to increase.

The synthesis of DNA with automated polymerase chain reaction protocols can generate a high concentration of DNA products. To detect specific DNA sequences within a product mixture, a responsive MRI contrast agent should show high specificity for the desired DNA sequence. For example, a dinuclear Nd(III) macrocyclic complex showed an increase in CEST when interacting with 0.5 mM of a specific DNA hairpin loop (106). The increase in CEST was attributed to an increase in the chemical exchange rate of the agent's amide groups that interacted with the DNA. Similarly, a Gd(III) chelate with a DNA ligand formed a DNA duplex with a specific complimentary sequence at 0.03 mM monomer concentration, causing a slower tumbling time of the agent that caused a decrease in the T_1 relaxation time constant (107). MR spectroscopy of hyperpolarized ^{129}Xe in a cryptophane cage with a DNA ligand can detect a specific complimentary DNA sequence through a change in the ^{129}Xe chemical shift (108). This last example exploited a modular design that represents a platform technology, which can be conveniently modified to target other specific DNA sequences. Athough these examples show the high creativity of this research field, the low concentration of DNA is a major limitation when detecting specific DNA sequences with these responsive MRI contrast agents.

4.4. Responsive MRI contrast agents that detect metabolites

The study of metabolism with MRI has greatly benefitted from the rapid development and use of hyperpolarized ^{13}C metabolites, including hydrogen peroxide and the enzyme

substrates listed in section 4.2 (109). Also, the rapid development of CEST MRI has provided opportunities to detect metabolites with labile protons, such as glucose, glutamate, myo-inositol, creatine, and hydrogen peroxide (110–115). Oxygen is a paramagnetic metabolite, which can directly affect the T_1 relaxation time constant of endogenous lipids (116) or exogenous ^{1}H and ^{19}F agents (117,118). Yet these methodologies directly detect a sub-population via hyperpolarized ^{13}C MRS/I or the metabolite population via CEST MRI, or assess the endogenous T_1 relaxation time constant affected by O_2, rather than detecting a change in a physicochemical characteristic that generates a change in imaging signal. Therefore, these approaches do not use responsive MRI contrast agents as defined in this review.

The development of responsive MRI contrast agents that directly detect metabolites has been limited during the last 8 years. Two Gd(III) chelates have been developed that reduce water access to the Gd(III) ion by forming a non-covalent adduct with sugars or pyrophosphate, which decreases water accessibility and increases T_1 relaxation time constant of the system (119,120). This reversible responsive agent is well suited for detecting sugars or pyrophosphate that have dynamic concentrations during the MRI acquisition period. Similarly, the binding of dopamine (Fig. 10; 121) or serotonin (122) to the heme group of an engineered protein reduces water accessibility to the iron of the heme, resulting in an increased T_1 relaxation time constant. The combination of protein engineering and biomedical imaging required to achieve this result exemplifies a clever multidisciplinary approach for molecular imaging. Using a different approach, the pendant alcohol groups of a paramagnetic CEST agent have chemical exchange rates that are too fast to generate CEST, but have slower chemical exchange rates that generate CEST when the alcohols interact with phosphate derivatives, thereby providing a means to detect phosphates (123). Many of these examples have limited specificity for detecting a single metabolite, primarily due to the similar compositions of many metabolites, which is a significant limitation for further developing this class of responsive MRI contrast agents.

4.5. Responsive MRI contrast agents that detect redox state

The reducing and oxidizing environments in tissues can affect disease states and biological processes (124,125). Redox state within cells, cell organelles, or the extracellular environment is often regulated by metabolites, including NADH, peroxides, glutathione, nitric oxide, and oxidase enzymes. Many of these redox-controlling metabolites can reduce or oxidize a responsive MRI contrast agent. However, a responsive agent's specificity for only one type of redox-controlling metabolite can be poor for some agents, and has not been demonstrated for other agents, suggesting that these responsive agents are detecting the redox state rather than a specific metabolite. In addition, oxygen is the eponymous example of an oxidizing agent, so that MRI contrast agents can be oxidized in hyperoxic conditions and reduced in hypoxic conditions. Yet some of these MRI contrast agents are directly responsive to the redox environment, and only indirectly responsive to oxygen status.

Because reduction causes a gain of electrons and oxidation causes a loss of electrons, perhaps the most straightforward design of a redox-sensitive MRI contrast agent involves a change in oxidation state of a free radical or a metal ion of the agent. For example, the

reduction of a paramagnetic nitroxide radical to a non-paramagnetic hydroxylamine lengthens the T_1 relaxation time constant, which was used to map redox state *in vivo* (Fig. 11; 126). A manganese chelate with a reduced Mn(II) form has been shown to generate strong T_1 relaxation resulting in a short T_1 relaxation time constant, while the oxidized Mn(III) state generates weak T_1 relaxation that creates a long T_1 relaxation time constant (127). A paramagnetic Co(II) chelate shows a strong CEST effect, but the corresponding oxidized Co(III) chelate is diamagnetic and does not generate CEST (128).

A change in electronic state of non-metallic components of a contrast agent can also be exploited to detect redox state. As a straightforward example, hyperpolarized [1-^{13}C]-dehydrascorbate can be reduced to vitamin C, which changes the ^{13}C chemical shift by 3.8 ppm (129). The incorporation of O_2 into a siloxane polymeric matrix causes a change in electronic state of the polymer, causing a decrease in T_1 relaxation time constant of the system (130). As a more complex example, a Eu(III) chelate with a N-methylquinolinium ligand (131) or an anthryl ligand (132) can be reduced, which causes a change in the electron density at the coordinating ligand. This change in electron density slows the chemical exchange rate of the water that coordinates the Eu(III) ion. Chemical exchange rates can cause the chemical shift of the labile hydrogen atom of CEST agent to become a weighted average of the chemical shifts of the hydrogen on water and on the agent (a phenomenon known as MR coalescence). Therefore, the change in chemical shift of this agent manifests as a change in the CEST effect, which reports on the reducing environment.

Reduction and oxidation can lead to a change in water accessibility of a metal chelate, which can change T_1 relaxation time constants. For example a manganese chelate can be oxidized by hydrogen peroxide to form a biomolecular product that blocks water access to the manganese ions, which increases the T_1 relaxation time constant of the system (133). Similarly, a Gd(III) chelate with a merocyanine motif that can be reduced to a spiropyran motif, which blocks water accessibility to the Gd(III) and causes the T_1 relaxation time constant to increase (134). Conversely, the reduction of a nitro group to form a protonated amino group forces the positively charged amino group to be repelled from the positively charged Gd(III) ion in the chelate, which decreases the T_1 relaxation time constant by increasing water accessibility to the Gd(III) ion (135). Increased water accessibility was also observed for oxidized Mn(III) in a porphyrin-containing protein, which decreased the T_1 relaxation time constant for this system relative to the reduced Mn(II) form of this agent (136).

Changing the tumbling time of the agent can also modulate T_1 relaxation. For example, a Gd(III) chelate with a thiol group can undergo oxidation and form a disulfide bond with the redox-sensitive Cys^{34} amino acid residue of albumin (137). The slowing of the tumbling time of the protein-bound Gd(III) chelate leads to a decrease in T_1 relaxation time constant. Notably, the binding of the agent to albumin may cause a decrease in water accessibility, leading to an increase in the T_1 relaxation time constant of the system. These offsetting effects may explain the reduced responsiveness to redox from this agent, which may compromise both sensitivity and specificity for detecting redox states.

4.6. Responsive contrast agents that detect metal ions

Ion transport in biological systems has been studied since the 19th century (138). Metal homeostasis emerged as important medical research field in the 1980s, especially regarding neurodegenerative diseases (139). More recently, the many dynamic roles of metals in functional biochemistry have spawned the field of metallomics (140). A variety of responsive MRI contrast agents have been developed to address the need to study metal ions within *in vivo* tissues. Care should be taken to design and use agents that measure the physiologically relevant concentration range for each desired metal ion, and that are sufficiently sensitive to measure changes in ion concentrations that pertain to the biomedical condition under study.

The most common mechanism for detecting metal ions with MRI is the use of contrast agents that change T_1 relaxation in response to a change in water accessibility to Gd(III). These contrast agents contain a ligand that coordinates the Gd(III) ion in a chelate, and the ligand then reorients away from the Gd(III) and binds to another metal ion, providing greater water accessibility to the Gd(III) ion that increases the T_1 relaxation time constant of the system. This mechanism has been exploited to detect Zn^{2+}, Ca^{2+}, Cu^{+}, or Cu^{2+}, by designing a ligand that has strong and specific binding to the desired metal (Fig. 12a; 141–146). A similar contrast agent that binds to Zn^{2+} exploits a different mechanism by subsequently binding to albumin, causing 3-fold decrease in T_1 relaxation time constant of the Zn^{2+}-albumin-bound agent (147, 148). These many examples demonstrate that this approach is a platform technology for detecting metal ions with MRI. Multiple ligands from the same contrast agent may dissociate from the Gd(III) and associate with the targeted metal ion, or multiple ligands from two tethered agents may reorient from Gd(III) to the targeted metal, which can improve the sensitivity of the MRI response from the agents. This same mechanism has been used to change the water accessibility of Mn(III) to detect Zn^{2+} (149). The coordination of ligands to a metal ion can also be designed to change water accessibility to the contrast agent. The pyridine ligands of a PARACEST agent can coordinate Zn^{2+} in an orientation that overlaps with the position of the bound water of the agent, which accelerates the exchange rate of this bound water and therefore causes a loss of CEST (Fig. 12b; 150). In general, the extensive use of chelation chemistry for detecting metal ions with responsive MRI contrast agents has naturally derived from the extensive development of metal chelates for MRI.

The extensive understanding of metal chelation has also driven the development of MRI contrast agents that change T_1 relaxation in response to a change in tumbling time. Three Gd(III) chelate contrast agents with a 1,10-phenanthroline ligand can coordinate Fe^{2+}, Ni^{2+}, or Mn^{n+}, creating a rigid trimer that tumbles more slowly than each monomer (151,152). Similarly, a Gd(III) chelate with a bisphosphate ligand can coordinate Ca^{2+} or Mg^{2+} ions, creating an oligomer that has a slower tumbling time (153). In addition, the coordination of a Gd(III) chelate to a metal can be followed by metal-induced binding to a protein, causing the protein-metal-bound Gd(III) chelate to tumble more slowly (149). In each case, the slower tumbling time leads to a decrease in the T_1 relaxation time constant of the system. An understanding of bioinorganic chemistry and biomedical imaging is needed to develop this

approach, which once again shows how multidisciplinary research is needed to develop novel responsive MRI contrast agents.

Achieving high specificity for detecting a single type of metal ion with this mechanism can be difficult, especially with systems that need coordination involving multiple molecules. To address this problem, a DNAzyme has been used to create a uranium-detecting MRI contrast agent (154). One DNA strand of the DNAzyme was conjugated to streptavidin, while the other strand was conjugated to a Gd(III) chelate, to create a macromolecular agent that creates a decreased T_1 reaxation time constant for the system. The binding of UO_2^{2+} to the DNAzyme causes the strand with the Gd(III) chelate to be cleaved and dissociate from the macromolecular complex, and the increase in tumbling time of the Gd(III) chelate causes an increase in the T_1 reaxation time constant. Although there may be no apparent need to detect uranium in biomedical systems with MRI, this example shows the high creativity of this research field, which may lead to the development of new agents that use a similar DNAzyme-based mechanism.

Responsive MRI contrast agents have been developed that take advantage of the ionic effects of metals. In particular, the chemical shift of hyperpolarized ^{129}Xe in a cryptophane cage is very sensitive to the electronic distribution of the cryptophane. The coordination of Zn^{2+} by a nitrolotriacetic acid ligand of the cryptophane cage causes a ~2 ppm change in the ^{129}Xe chemical shift (155). As another example, a phenylboronic acid-pendant cyclen can chelate Zn^{2+} that balances the charges in the system, which catalyzes the hydrolysis of the ligands to release boronic acid and causes a change in the chemical shift of ^{11}B (156). PARACEST agents can also be sensitive to electronic redistributions caused by ionic effects of metals. The coordination of bis-carboxylate ligands to Ca^{2+} causes an electronic redistribution in a PARACEST agent, resulting in a 10-fold reduction in chemical exchange rate and a loss of CEST (157).

4.7. Responsive contrast agents that measure pH

The measurement of extracellular pH has significant clinical value for disease diagnoses (158), for predicting the efficacy of pH-dependent chemotherapies (159), and for monitoring the effects of pH-altering therapies (160). For example, the extracellular pH in solid tumors typically ranges between ~6.5 and ~7.2, which requires pH measurements with excellent accuracy and precision to assess tumor acidosis in this narrow pH range. The measurement of intracellular pH provides outstanding opportunities to monitor the endosomal pathway for drug delivery (161). The evolution of immature endosomes to mature lysosomes is marked by an evolution from a neutral pH of ~7 to an acidic pH of ~5. Therefore, monitoring this evolution requires pH measurements with moderate accuracy and precision, and can be monitored with agents that are responsive to pH transitions rather than requiring accurate pH measurements.

Acidification is commonly employed to dissolve or degrade materials. This approach has been employed to dissolve urchin shaped nanoparticles or hollow mesoporous silica nanoparticles containing manganese, which releases the manganese and decreases the T_1 relaxation time constant of the system (162,163). Similarly, acidification of a pH-sensitive liposome causes release of a Gd(III) chelate into solution and decreases the T_1 relaxation

time constant (164). Acidification of a imidazole-containing micelle that encapsulates Gd(III) chelates can cause the micelle to disassemble and decrease the T_1 relaxation time constant of the system, which has been used to diagnose acidic tumors during *in vivo* studies (165). Hydrogels can also be acidified, which swells the hydrogel and releases coated SPIONs into the surrounding water that decrease the T_2* relaxation time constant (166). A polymeric micelle with a polyaminoester component can also be acidified, which dissolves the micelles and releases uncoated SPIONs (167). However, unlike coated SPIONs that are soluble, uncoated SPIONs rapidly precipitate, which increases the T_2* relaxation time constant. Each of these systems relies on dissociation of the metal from an agent, and are therefore irreversible responsive MRI contrast agents. Each of these systems is responsive to a pH transition, but cannot accurately measure the pH.

A change to a more acidic pH can protonate a MRI contrast agent, leading to a change in tumbling time that changes T_1 relaxation. For example, increased protonation of a cross-linked polymer embedded with carboxylate groups and flexible Gd(III) chelates causes the polymer to shrink, which reduces the flexibility of the Gd(III) chelates and decreases the T_1 relaxation time constant of the system (168). This macroscopic system has a large number of carboxylate groups that create a near-continuous range of protonation states, which creates a near-continuous scale for measuring pH. Each protonation event is reversible, so that this MRI contrast agent is reversibly responsive.

A change in protonation state can also be exploited to change water accessibility of the agent, which leads to a change in T_1 relaxation. An aminoethyl group of a chelate can coordinate to a Gd(III) ion, blocking the water accessibility to the Gd(III) and causes the T_1 relaxation time constant to increase (169). An increased propensity for protonation of the aminoethyl group at acidic pH causes this group to dissociate from the Gd(III), providing accessibility for water to the Gd(III) and decreasing T_1 relaxation time constant. Similarly, a mesitylene-based ligand blocks water access to Gd(III) in a HOPO-based chelate. Protonation of this ligand causes charge-charge repulsion with the Gd(III) ion, forcing the ligand away from Gd(III) which allows water to interact with Gd(III) that causes a decrease in T_1 relaxation time constant (170). These agents are reversibly responsive, and can measure pH values.

Chemical exchange between water and an amide or amine group is base-catalyzed at physiological pH. Therefore, the amplitude of CEST is dependent on pH. Although other conditions can change the CEST amplitude, including the concentration of the agent, CEST agents that have two selectively detectable CEST effects can be used to measure a concentration-independent ratio of CEST that is still dependent on pH. In addition, fast chemical exchange rates change the chemical shift of the detected CEST through the effect of MR coalescence. Furthermore, some CEST agents can have two conformations that generate CEST at different chemical shifts. Rapid interconversion between these conformations creates one chemical shift at the population-weighted average of the chemical shifts of the two conformers. The pH can alter the relative populations of the two conformers, thereby altering the weighted-average chemical shift of the CEST effect. Thus a pH-dependent change in chemical exchange rate can also change the chemical shift of CEST. The chemical shift is independent of concentration, which improves the utility of this

technique. Therefore, many CEST agents have been developed to measure pH, including PARACEST agents (171–176) and DIACEST agents (177,178), and some of these CEST agents have been used to measure extracellular pH within *in vivo* tumors (Fig. 13). The chemical shift of a hyperpolarized ^{89}Y chelate has also been shown to be sensitive to pH, and therefore can also measure pH values (46).

4.8. Responsive contrast agents that measure temperature

Chronic hyperthermia can be used to treat tumors and other pathological tissues, and acutely heating tissues has been used to release drug payloads from thermosensitive nanocarriers (179,180). Non-invasive monitoring of tissue temperature can be used ensure that temperature-based treatments are localized to pathological tissues. A variety of MRI techniques have been used to map temperature distributions in tissues, including MRS and MRI phase mapping of the temperature-dependent chemical shift of water, and MRI to measure the temperature-dependent T_1 relaxation time constant and diffusion rate of water (181). Yet MR signal phases, chemical shifts, T_1 relaxation time constants and diffusion rates depend on other tissue characteristics, which may compromise the accuracy of the temperature map.

Responsive MRI contrast agents have also been developed to measure temperature maps. The concept of thermosensitive drug nanocarriers has been leveraged to make thermosensitive liposomes that can be heated to release a Gd(III)-based MRI contrast agent, which improves the water accessibility of the agent and decreases T_1 relaxation time constant (182). Liposomes that are tuned to transition from gel to liquid crystalline phases at specific temperatures can be used to measure temperature transitions. DNA duplexes are also thermosensitive, as complimentary DNA strands can be designed to dissociate at specific temperatures. SPIONs can be aggregated when their DNA ligands associate to form a network of duplexes, which can be disaggregated at higher temperatures that cause the DNA strands to dissociate (105). This reversible disaggregation causes an increase in T_2* relaxation time constant, which can be used to measure temperature transitions. Solid gadolinium metal is also thermosensitive, transitioning from a ferromagnetic state to a paramagnetic state at the Curie temperature (183). A loss in magnetic susceptibility caused by transitioning to the paramagnetic state can be used to measure temperature transitions.

Dy(III) and Eu(III) chelates with Gly and GlyPhe amino acid ligands or t-butyl amide ligands can generate a temperature-dependent CEST effect, because chemical exchange rates are dependent on temperature (Fig. 14; 175,184–186). A temperature-dependent change in chemical exchange rate can also change the chemical shift of CEST through the effect of MR coalescence. The temperature-dependent change in amplitude of the CEST effect is typically greater than the change in chemical shift, which has advantages regarding measurement precision. Yet the chemical shift measurement is independent of other conditions such as concentration of the agent or the endogenous T_1 relaxation time constant of the tissue, which has advantages regarding measurement accuracy.

4.9. Responsive contrast agents that detect light

Bioluminescence is a very unique characteristic of some biological systems that has been exploited for many diagnostic applications in biomedicine. The fluorescence of many proteins can be stimulated by a light source outside the biological system, while light can be generated from within a biological system from the catalysis of luciferin by luciferase, or via Cerenkov radiation (187–189). However, light scattering and absorbance in tissues can reduce the spatial resolution and depth of tissues that may be interrogated during diagnostic tests. To address these pitfalls, responsive MRI contrast agents have recently been developed that can detect light. A Gd(III) chelate with a merocyanine motif can be converted to a spiropyran motif with light at 563 nm wavelength, which increases water accessibility to the Gd(III) and decreases the T_1 relaxation time constant (Fig. 15; 134). This same hydrophilic merocyanine motif was conjugated to SPIONs, and light-induced conversion to a hydrophobic spiropyran motif caused the nanoparticles to aggregate and increase their superparamagnetism, leading to a decrease in T_2* relaxation time constant (190). These last examples attest to the creativity of this research field with responsive MRI contrast agents. Such creativity may provide opportunities to detect and measure other environmental conditions, such as flow, hydrophobicity, or pressure.

5. Future Directions

The combination of our previous review (17) and our current review has uncovered a total of 171 examples of responsive MRI contrast agents (Fig. 16). Approximately one third of these agents detect enzyme activity, one third detect pH or ions, and one third detect the remaining biomarkers. This distribution has been consistent between the two reviews, with only a minor increase in the development of redox-responsive agents and a minor decrease in developing metabolite-responsive agents and contrast agents that measure pH. The development of platform technologies for detecting some classes of biomarkers is partly reflected by this distribution. The relatively few examples of responsive MRI contrast agents for some biomarker categories demonstrate an area of unmet need for future research endeavors.

As a general consideration, the detection sensitivity of responsive MRI contrast agents is often low, which often compromises the ability to detect or quantify the molecular biomarker that is interrogated by the agent. Furthermore, many hurdles involved with *in vivo* pharmacokinetics can reduce the delivery of contrast agents to tissues that harbor a molecular biomarker. Nanocarriers may potentially be used to address these two potential pitfalls, including linear polymers, branched polymers, proteins, micelles, liposomes, and hydrogels (191). A payload of tens-to-thousands of MRI contrast agent molecules may be packaged in these nanocarriers, which can greatly amplify detection sensitivity. Nanocarriers may also improve delivery of the agent to tissues. This improved delivery may occur through passive mechanisms, such as using nanoparticles that exploit the Enhanced Permeability and Retention effect exhibited by some solid tumors, or such as PEGylating the surface of the nanocarrier to avoid uptake of the agent in the nanocarrier by the reticuloendothelial system. This improved delivery may also occur through active

mechanisms, such as coating the nanocarrier with ligands that provide avidity for uptake in specific tissues.

As shown by some examples highlighted in this review, the disassembly or disaggregation of a nanocarrier can change the physicochemical properties of a responsive MRI contrast agent associated with the nanocarrier. In these cases, the nanocarrier is an inherent component of the response mechanism. For responsive MRI contrast agents that are not inherently dependent on the nanocarrier, care should be taken to ensure that responsive MRI contrast agents that are packaged in nanocarriers do not lose their responsiveness. This loss of response may occur by shielding the agent from the environment that contains the intended molecular biomarker, or by partially quenching the response of each agent by placing the agents in close proximity. Some evidence has shown that this quenching effect may be particularly problematic for some CEST agents that are packaged with a nanocarrier.

Clinical MRI scanners are now available with 7T “ultra high” magnetic field strengths, and pre-clinical MRI scanners have been developed with 15.2 T ultra-high magnetic fields (192). Stronger magnetic fields improve the dynamic range of chemical shifts in absolute units of Hz, which can improve the precision of measuring chemical shifts. CEST and MRS/I acquisition methods can measure chemical shifts, so that ultra-high magnetic fields may improve the precision of detecting molecular biomarkers with responsive CEST and MRS/I contrast agents. In addition, a CEST agent must have a chemical shift relative to water in absolute units of Hz that does not exceed the chemical exchange rage that is also represented in units of Hz. Expanding the chemical shift of the agent to greater values in Hz provides the opportunity to generate CEST with agents that have faster chemical exchange rates. Therefore, ultra-high magnetic fields may potentially expand the variety of CEST agents that can respond to molecular biomarkers.

The availability of ultra-high magnetic fields may have less impact on the development of responsive MRI contrast agents that employ T_1- and T_2*-relaxation. The relaxivities of T_1 contrast agents typically decrease in ultra-high magnetic fields. Yet T_1 contrast agents still have value at these field strengths, because the T_1 relaxation time constant of the endogenous tissue becomes longer in ultra-high magnetic fields. Thus a small change in T_1 relaxation time constant caused by an agent in tissue with a long endogenous T_1 relaxation time constant in ultra-high magnetic fields may be just as easy to measure as a large change in T_1 relaxation time constant caused by the agent in tissue with a short endogenous T_1 relaxation time constant in weaker magnetic fields. T_2* contrast agents may have less value in ultra-high magnetic fields, because the magnetic field inhomogeneities within endogenous tissues are accentuated at higher magnetic fields. The relaxivities of T_2* contrast agents are primarily independent of the magnetic field strength, and instead depend on the local magnetic field inhomogeneities imposed by the agent, so that a higher magnetic field strength does not improve the responsiveness of these agents (27). Thus, the change in T_2* relaxation time constant caused by a contrast agent may be more difficult to assess if the endogenous T_2* relaxation time constant is very short.

Many examples of reporter gene imaging have employed responsive contrast agents (193). Both β-galactosidase and β-lactamase have often been used as reporter gene systems for

optical imaging, which has led to an abundance of responsive MRI contrast agents that detect these enzyme activities. Yet other responsive MRI contrast agents may possibly be used for reporter gene imaging. A protein produced by transcription and translation of the reporter gene may possibly change the concentration of DNA, metabolites, or ions surrounding a responsive MRI contrast agent, or may possibly change the pH, redox state, temperature or luminescence near the vicinity of the responsive agent. Exploiting these other responsive MRI contrast agents may expand reporter gene imaging. As an example, the detection of a polyphosphate metabolite with ^{31}P MRS has been exploited for reporter gene imaging (194).

Many examples of responsive MRI contrast agents listed in this review have shown the merits of a multidisciplinary approach that includes cellular and molecular biology. Reporter gene imaging is an outstanding example that inherently requires an understanding of genetic expression processes and biochemical pathways in cell biology. Additional multistep mechanisms have also been employed to develop responsive MRI contrast agents, such as protein-protein interactions, cell-cell signaling, cell trafficking, and biological processes of organelles. Therefore, multidisciplinary research that combines cell and molecular biology with radiology and chemistry has great potential to provide innovation for developing additional responsive MRI contrast agents. This review provides a foundation for developing these multidisciplinary approaches that can expand the armamentarium of molecular imaging.

Conclusion

This review evaluated 117 examples of responsive MRI contrast agents that have been reported between 2005 and 2014, which adds to the 54 examples that were previously reported. This increase in the number of agents within the last eight years reflects the growing interest in developing new MRI methods for molecular imaging. The changes in six physicochemical characteristics of MRI contrast agents have been exploited to detect concentrations or activities of enzymes, proteins, nucleic acids, metabolites, or metal ions, and changes in redox state, pH, temperature, or light. These many combinations of physicochemical characteristics and biomarkers show the outstanding creativity that drives this research field.

Supplementary Material

Refer to Web version on PubMed Central for supplementary material.

Acknowledgments

This work was supported by the Phoenix Friends of the Arizona Cancer Center, and NIH grants R01 CA169774-01 and P50 CA95060, DVH was sponsored by the TRIF Fellowship Program of the University of Arizona. doi: 10.1038/nm1208

References

1. Lauterbur PC. All science is interdisciplinary – From magnetic moments to molecules to men (Nobel lecture). Angew Chemie Int Ed. 2005; 44(7):1004–1011.10.1002/anie.200462400

2. Smith-Bindman R, Miglioretti DL, Johnson E, Lee C, Feigelson HS, Flynn M, Greenlee RT, Kruger RL, Hornbrook MC, Roblin D, Solberg LI, Vanneman N, Weinmann S, Williams AE. Use of diagnostic imaging studies and associated radiation exposure for patients enrolled in large integrated health care systems, 1996–2010. J Am Med Assoc. 2012; 307(22):2400–2409.10.1001/jama.2012.5960

3. Organisation for Economic Co-operation and Development. Health at a glance 2011: OECD indicators. OECD Publishing; Paris, France: 2011.

4. Young IR, Clarke GJ, Bailes DR, Pennock JM, Doyle FH, Bydder GM. Enhancement of relaxation rate with paramagnetic contrast agents in NMR imaging. J Comput Tomogr. 1981; 5(6):543–547. [PubMed: 7053127]

5. Brady TJ, Goldman MR, Pykett IL, Buonanno FS, Kistler JP, Newhouse JH, Burt CT, Hinshaw WS, Pohost GM. Proton nuclear magnetic resonance imaging of regionally ischemic canine hearts: Effect of paramagnetic proton signal enhancement. Radiol. 1982; 144(2):343–347.

6. Goldman MR, Grady TJ, Pykett IL, Burt CT, Buonanno FS, Kistler JP, Newhouse JH, Hinshaw WS, Pohost GM. Quantification of experimental myocardial infarction using nuclear magnetic resonance imaging and paramagnetic ion contrast enhancement in excised canine hearts. Circulation. 1982; 66(5):1012–1016.10.1161/01.CIR.66.5.1012 [PubMed: 6181904]

7. Brasch RC, Nitecki DE, Brant-Zawadzki M, Enzmann DR, Wesbey GE, Tozer TN, Tuck LD, Cann CE, Fike JR, Sheldon P. Brain nuclear magnetic resonance imaging enhanced by a paramagnetic nitroxide contrast agent: preliminary report. Am J Roentgen. 1983; 141(5):1019–1023.10.2214/ajr.141.5.1019

8. Wesbey G, Engelstad B, Lipton M, Brasch R, Weinmann H, Higgins C, Sievers R. Myocardial NMR imaging employing gadolinium-DTPA. Magn Reson Med. 1984; 1(2):287.10.1002/mrm.1910010206

9. Carr DH, Brown J, Bydder GM, Weinmann HJ, Speck U, Thomas DJ, Young IR. Intravenous chelated gadolinium as a contrast agent in NMR imaging of cerebral tumours. Lancet. 1984; 1(8375):484–486.10.1016/S0140-6736(84)92852-6 [PubMed: 6142210]

10. Major JL, Meade TJ. Bioresponsive, cell-penetrating, and multimeric MR contrast agents. Acc Chem Rev. 2009; 42(7):893–903.10.1021/ar800245h

11. Giesel FL, Mehndiratta A, Essig M. High-relaxivity contrast-enhanced magnetic resonance neuroimaging: a review. Eur Radiol. 2010; 20(10):2461–74.10.1007/s00330-010-1805-8 [PubMed: 20567832]

12. Saeed M. New concepts in characterization of ischemically injured myocardium by MRI. Exp Biol Med. 2001; 226(5):367–376.

13. Edelman RR, Mattle HP, Atkinson DJ, Hill T, Finn JP, Mayman C, Ronthal M, Hoogewoud HM, Kleefield J. Cerebral blood flow: assessment with dynamic contrast-enhanced T2*-weighted MR imaging at 1.5T. Radiol. 1990; 176(1):211–220.

14. Prince MR. Gadolinium enhanced MR aortography. Radiol. 1994; 191:155–164.

15. Yankeelov TE, Gore JC. Dynamic contrast enhanced magnetic resonance imaging in oncology: theory, data acquisition, analysis, and examples. Curr Med Imaging Rev. 2007; 3(2):91–107. [PubMed: 19829742]

16. Weissleder, R.; Ross, BD.; Rehemtulla, A.; Gambhir, SS. Molecular Imaging: Principles and Practice. People's Medical Publishing House; Shelton CT: 2010.

17. Yoo B, Pagel MD. An overview of responsive MRI contrast agents for molecular imaging. Front Biosci. 2008; 13:1733–1752.10.2741/2796 [PubMed: 17981664]

18. Gallez B, Lacour V, Demeure R, Debuyst R, Dejehet F, De Keyser JL, Dumont P. Spin labeled arabinogalactan as MRI contrast agent. Magn Reson Imaging. 1994; 12(1):61–69.10.1016/0730-725X(94)92353-1 [PubMed: 8295509]

19. Lancelot E, Amirbekian V, Brigger I, Raynaud JS, Ballet S, David C, Rousseaux O, Le Greneur S, Port M, Lijnen HR, Bruneval P, Michel JB, Ouimet T, Roques B, Amirbekian S, Hyafil F, Vucic E, Aguinaldo JG, Corot C, Fayad ZA. Evaluation of matrix metalloproteinases in atherosclerosis using a novel noninvasive imaging approach. Arterioscler Thromb Vasc Biol. 2008; 28(3):425–432.10.1161/ATVBAHA.107.149666 [PubMed: 18258820]

20. Prantner AM, Sharma V, Garbow JR, Piwnica-Worms D. Synthesis and characterization of a Gd-DOTA-D-permeation peptide for magnetic resonance relaxation enhancement of intracellular targets. Molec Imaging. 2003; 2(4):333–341. [PubMed: 14717332]
21. Genove G, DeMarco U, Xu H, Goins WF, Ahrens ET. A new transgenic reporter for *in vivo* magnetic resonance imaging. Nat Med. 2005; 11:450–454.10.1038/nm1208 [PubMed: 15778721]
22. Artemov D. Molecular magnetic resonance imaging with targeted contrast agents. J Cell Biochem. 2003; 90(3):518–524.10.1002/jcb.10660 [PubMed: 14523986]
23. Islam T, Josephson L. Current state and future applications of active targeting in malignancies using superparamagnetic iron oxide nanoparticles. Cancer Biomarkers. 2009; 5(2):99–107.10.3233/CBM-2009-0615 [PubMed: 19414927]
24. Moats RA, Fraser SE, Meade TJ. A “smart” magnetic resonance imaging agent that reports on specific enzymic activity. Angew Chemie Int Ed. 1997; 36(7):726–728.10.1002/anie.199707261
25. Nivorozhkin AL, Kolodziej AF, Caravan P, Greenfield MT, Lauffer RB, McMurry TJ. Enzyme-activated Gd3+ magnetic resonance imaging contrast agents with a prominent receptor-induced magnetization enhancement. Angew Chemie Int Ed. 2001; 40(15):2903–2906.10.1002/1521-3773
26. Haacke, EM.; Brown, RW.; Thompson, MR.; Venkatesan, R. Magnetic Resonance Imaging: Physical Principles and Sequence Design. John Wiley & Sons; New York: 1999.
27. Merbach, A.; Toth, E. The chemistry of contrast agents in medical magnetic resonance imaging. 1. John Wiley & Sons; New York: 2001.
28. Ahrens ET, Rothbacher U, Jacobs RE, Fraser SE. A model for MRI contrast enhancement using T1 agents. Proc Natl Acad Sci USA. 1998; 95:8443–8448. [PubMed: 9671697]
29. Stuber M, Gilson WD, Schar M, Kedziorek DA, Hofmann LV, Shah S, Vonken E, Bulte JWM, Kraitchman DL. Positive contrast visualization of iron oxide-labeled stem cells using inversion recovery with ON-resonant water suppression (IRON). Magn Reson Med. 2007; 58:1072–1077.10.1002/mrm.21399 [PubMed: 17969120]
30. Pike MM, Stoops CN, Langford CP, Akella NS, Nabors LB, Gillespie GY. High-resolution longitudinal assessment of flow and permeability in mouse glioma vasculature: sequential small molecule and SPIO dynamic contrast agent MRI. Magn Reson Med. 2009; 61:615–625.10.1002/mrm.21931 [PubMed: 19235262]
31. Mills PH, Ahrens ET. Theoretical MRI contrast model for exogenous T2 agents. Magn Reson Med. 2007; 57(2):442–447.10.1002/mrm.21145 [PubMed: 17260382]
32. Ward KM, Aletras AH, Balaban RS. A new class of contrast agents for MRI based on proton chemical exchange dependent saturation transfer (CEST). J Magn Reson. 2000; 143(1):79–87.10.1006/jmre.1999.1956 [PubMed: 10698648]
33. McMahon MT, Gilad AA, DeLiso MA, Berman SM, Bulte JW, van Zijl PC. New “multicolor” polypeptide diamagnetic chemical exchange saturation transfer (DIACEST) contrast agents for MRI. Magn Reson Med. 2008; 60(4):803–812.10.1002/mrm.21683 [PubMed: 18816830]
34. Zhang S, Merritt M, Woessner DE, Lenkinski RE, Sherry AD. PARACEST agents: modulating MRI contrast via water proton exchange. Acc Chem Res. 2003; 36(10):783–790.10.1021/ar020228m [PubMed: 14567712]
35. Dorazio SJ, Morrow JR. Iron(II) complexes containing octadentate tetraazamacrocycles as paraCEST magnetic resonance imaging contrast agents. Inorg Chem. 2012; 51(14):7448–7450.10.1021/ic301001u [PubMed: 22757664]
36. Olatunde AO, Dorazio SJ, Spernyak JA, Morrow JR. The NiCEST approach: nickel(II) paraCEST MRI contrast agents. J Am Chem Soc. 2012; 134(45):18503–18505.10.1021/ja307909x [PubMed: 23102112]
37. Cárdenas-Rodríguez J, Howison CM, Matsunaga TO, Pagel MD. A reference agent model for DCE MRI can be used to quantify the relative vascular permeability of two MRI contrast agents. Magn Reson Imaging. 2013; 31:900–910.10.1016/j.mri.2012.12.002. [PubMed: 23583323]
38. Holloway C, ten Hove M, Clarke K, Neubauer S. MR spectroscopy in heart failure. Front Biosci (Schol Ed). 2011; 3:331–340. [PubMed: 21196379]
39. Marino S, Ciurleo R, Bramanti P, Federico A, De Stefano N. 1H-MR spectroscopy in traumatic brain injury. Neurocrit Care. 2011; 14(1):127–33.10.1007/s12028-010-9406-6 [PubMed: 20737247]

40. Bolan PJ, Nelson MT, Yee D, Garwood M. Imaging in breast cancer: magnetic resonance spectroscopy. Breast Cancer Res. 2005; 7(4):149–52.10.1186/bcr1202 [PubMed: 15987466]
41. Yu JX, Kodibagkar VD, Cui W, Mason RP. ^{19}F: a versatile reporter for non-invasive physiology and pharmacology using magnetic resonance. Curr Med Chem. 2005; 12(7):819–48.10.2174/0929867053507342 [PubMed: 15853714]
42. Bendel P. Biomedical applications of ^{10}B and ^{11}B NMR. NMR Biomed. 2005; 18(2):74–82.10.1002/nbm.886 [PubMed: 15770608]
43. Ki S, Sugihara F, Kasahara K, Tochio H, Okada-Marubayashi A, Tomita S, Morita M, Ikeguchi M, Shirakawa M, Kokubo T. A novel magnetic resonance-based method to measure gene expression in living cells. Nucleic Acids Res. 2006; 34(6):e51.10.1093/nar/gkl135 [PubMed: 16598072]
44. Kurhanewicz J, Bok R, Nelson SJ, Vigneron DB. Current and potential applications of clinical ^{13}C MR spectroscopy. J Nucl Med. 2008; 49(3):341–344.10.2967/jnumed.107.045112 [PubMed: 18322118]
45. Taratula O, Dmochowski IJ. Functionalized ^{129}Xe contrast agents for magnetic resonance imaging. Curr Opin Chem Biol. 2010; 14(1):97–104.10.1016/j.cbpa.2009.10.009 [PubMed: 19914122]
46. Jindal AK, Merritt ME, Suh EH, Malloy CR, Sherry AD, Kovacs Z. Hyperpolarized ^{89}Y complexes as pH sensitive NMR probes. J Am Chem Soc. 2010; 132(6):1784–1785.10.1021/ja910278e [PubMed: 20102196]
47. Li W, Parigi G, Fragai M, Luchinat C, Meade TJ. Mechanistic studies of a calcium-dependent MRI contrast agent. Inorg Chem. 2002; 41(15):4018–4024.10.1021/ic0200390 [PubMed: 12132928]
48. Liu G, Li Y, Pagel MD. Design and characterization of new irreversible responsive PARACEST MRI contrast agent that detects nitric oxide. Magn Reson Med. 2007; 58:1249–1256.10.1002/mrm.21428 [PubMed: 18046705]
49. Frullano L, Catana C, Benner T, Sherry AD, Caravan P. Bimodal MR-PET agent for quantitative pH imaging. Angew Chem Int Ed. 2010; 49(13):2382–2384.10.1002/anie.201000075
50. Martinez GV, Zhang X, García-Martín ML, Morse DL, Woods M, Sherry AD, Gillies RJ. Imaging the extracellular pH of tumors by MRI after injection of a single cocktail of T_1 and T_2 contrast agents. NMR Biomed. 2011; 24(10):1380–1391.10.1002/nbm.1701 [PubMed: 21604311]
51. Yoo B, Sheth VR, Howison CM, Douglas MJK, Pineda CT, Maine EA, Baker AF, Pagel MD. Detection of *in vivo* enzyme activity with catalyCEST MRI. Mag Reson Med. 2014; 71:1221–1230.10.1002/mrm.24763.
52. Yoo B, Sheth V, Pagel MD. An amine-derivatized, DOTA-loaded polymeric support for FMOC solid phase peptide synthesis. Tet Lett. 2009; 50:4459–4462.10.1016/j.tetlet.2009.05.061
53. Suchy M, Ta R, Li A, Wojciechowski F, Pasternak SH, Bartha R, Hudson RHE. A paramagnetic chemical exchange-based MRI probe metabolized by cathepsin D: design, synthesis and cellular uptake studies. Org Biomolec Chem. 2010; 8(11):2560–2566.10.1039/b926639a
54. Hingorani DV, Randtke EA, Pagel MD. A catalyCEST MRI contrast agent that detects the enzyme-catalyzed creation of a covalent bond. J Am Chem Soc. 2013; 135(17):6396–6398.10.1021/ja400254e [PubMed: 23601132]
55. Chauvin T, Durand P, Bernier M, Meudal H, Doan B-T, Noury F, Badet B, Beloeil JC, Tóth E. Detection of enzymatic activity by PARACEST MRI: a general approach to target a large variety of enzymes. Angew Chemie Int Ed. 2008; 47(23):4370–4372.10.1002/anie.200800809
56. Li Y, Sheth VR, Liu G, Pagel MD. A self-calibrating PARACEST MRI contrast agent that detects esterase enzyme activity. Contrast Media Molec Imaging. 2011; 6(4):219–228.10.1002/cmmi.421 [PubMed: 21861282]
57. Liu G, Liang Y, Bar-Shir A, Chan KWY, Galpoththawela CS, Bernard SM, Tse T. Monitoring enzyme activity using a diamagnetic chemical exchange saturation transfer magnetic resonance imaging contrast agent. J Am Chem Soc. 2011; 133(41):16326–16329.10.1021/ja204701x [PubMed: 21919523]
58. Airan RD, Bar-Shir A, Liu G, Pelled G, McMahon MT, van Zijl PCM, Bulte JWM, Gilad AA. MRI biosensor for protein kinase A encoded by a single synthetic gene. Magn Reson Med. 2012; 68(6):1919–1923.10.1002/mrm.24483 [PubMed: 23023588]

59. Chang YT, Cheng CM, Su YZ, Lee WT, Hsu JS, Liu GC, Cheng TL, Wang YM. Synthesis and characterization of a new bioactivated paramagnetic gadolinium (III) complex [Gd (DOTA-FPG) (H2O)] for tracing gene expression. Bioconjug Chem. 2007; 18(6):1716–1727.10.1021/bc070019s [PubMed: 17935289]
60. Rodriguez E, Nilges M, Weissleder R, Chen JW. Activatable magnetic resonance imaging agents for myeloperoxidase sensing: mechanism of activation, stability, and toxicity. J Am Chem Soc. 2010; 132:168–177.10.1021/ja905274f [PubMed: 19968300]
61. Chen YJ, Wu SC, Chen CY, Tzou SC, Cheng TL, Huang YF, Yuan SS, Wang YM. Peptide-based MRI contrast agent and near-infrared fluorescent probe for intratumoral legumain detection. Biomaterials. 2014; 35:304–315.10.1016/j.biomaterials.2013.09.100 [PubMed: 24120038]
62. Querol M, Bennett DG, Sotak C, Kang HW, Bogdanov A Jr. A paramagnetic contrast agent for detecting tyrosinase activity. ChemBioChem. 2007; 8(14):1637–1641.10.1002/cbic.200700157 [PubMed: 17694521]
63. Arena F, Singh JB, Gianolio E, Stefanìa R, Aime S. β-Gal gene expression MRI reporter in melanoma tumor cells. Design, synthesis, and *in vitro* and *in vivo* testing of a Gd(III) containing probe forming a high relaxivity, melanin-like structure upon β-Gal enzymatic activation. Bioconjug Chem. 2011; 22(12):2625–2635.10.1021/bc200486j [PubMed: 22035020]
64. Cao CY, Shen YY, Wang JD, Liang GL. Controlled intracellular self-assembly of gadolinium nanoparticles as smart molecular MR contrast agents. Sci Reports. 2013; 3:1–9.10.1038/srep01024
65. LePage M, Dow WC, Melchior M, You Y, Fingleton B, Quarles CC, Pépin C, Gore JC, Matrisian LM, McIntyre JO. Noninvasive detection of matrix metalloproteinase activity *in vivo* using a novel magnetic resonance imaging contrast agent with a solubility switch. Mol Imaging. 2007; 6(6):393–403. [PubMed: 18053410]
66. Jastrzebska B, Lebel R, Therriault H, McIntyre JO, Escher E, Guerin B, Paquette B, Neugebauer WA, Lepage M. New enzyme-activated solubility-switchable contrast agent for magnetic resonance imaging: from synthesis to *in vivo* imaging. J Med Chem. 2009; 52(6):1576–1581.10.1021/jm801411h [PubMed: 19228016]
67. Himmelreich U, Aime S, Hieronymus T, Justicia C, Uggeri F, Zenke M, Hoehn M. A responsive MRI contrast agent to monitor functional cell status. NeuroImage. 2006; 32(3):1142–1149.10.1016/j.neuroimage.2006.05.009 [PubMed: 16815042]
68. Zhang HW, Wang LQ, Xiang QF, Zhong Q, Chen LM, Xu CX, Xiang XH, Xu B, Meng B, Wan YQ, Deng DYB. Specific lipase-responsive polymer-coated gadolinium nanoparticles for MR imaging of early acute pancreatitis. Biomaterials. 2014; 35:356–367.10.1016/j.biomaterials.2013.09.046 [PubMed: 24103651]
69. Figueiredo S, Moreira JN, Geraldes CFGC, Aime S, Terreno E. Supramolecular protamine/Gd-loaded liposomes adducts as relaxometric protease responsive probes. Bioorg Med Chem. 2011; 19:1131–1135.10.1016/j.bmc.2010.07.057 [PubMed: 20719523]
70. Giardiello M, Lowe MP, Botta M. An esterase-activated magnetic resonance contrast agent. Chem Comm. 2007; 44(39):4044–4046.10.1039/B711989E [PubMed: 17912410]
71. Napolitano R, Pariani G, Fedeli F, Baranyai Z, Aswendt M, Aime S, Gianolio E. Synthesis and relaxometric characterization of a MRI Gd-based probe responsive to glutamic acid decarboxylase enzymatic activity. J Med Chem. 2013; 56(6):2466–2477.10.1021/jm301831f [PubMed: 23469759]
72. Rolla GA, Tei L, Fekete M, Arena F, Gianolio E, Botta M. Responsive Mn(II) complexes for potential applications in diagnostic magnetic resonance imaging. Bioorg Med Chem. 2011; 19:1115–1122.10.1016/j.bmc.2010.07.064 [PubMed: 20801660]
73. Cui W, Liu L, Kodibagkar VD, Mason RP. S-Gal, a novel 1H MRI reporter for beta-galactosidase. Magn Reson Med. 2010; 64(1):65–71.10.1002/mrm.22400 [PubMed: 20572145]
74. Bengtsson NE, Brown G, Scott EW, Walter GA. lacZ as a genetic reporter for real-time MRI. Magn Reson Med. 2010; 63(3):745–753.10.1002/mrm.22235 [PubMed: 20146234]
75. Shapiro MG, Szablowski JO, Langer R, Jasanoff A. Protein nanoparticles engineered to sense kinase activity in MRI. J Am Chem Soc. 2009; 131(7):2484–2486.10.1021/ja8086938 [PubMed: 19199639]

76. Granot D, Shapiro EM. Release activation of iron oxide nanoparticles: (REACTION) a novel environmentally friendly MRI paradigm. Magn Reson Med. 2011; 65(5):1253–1259.10.1002/mrm.22839 [PubMed: 21360745]
77. Matsumura S, Aoki I, Saga T, Shiba K. A tumor-environment-responsive nanocarrier that evolves its surface properties upon sensing matrix metalloproteinase-2 and initiates agglomeration to enhance T2 relaxivity for magnetic resonance imaging. Molec Pharmaceutics. 2011; 8:1970–1974.10.1021/mp2001999
78. Schellenberger E, Rudloff F, Warmuth C, Taupitz M, Hamm B, Schnorr J. Protease-specific nanosensors for magnetic resonance imaging. Bioconjug Chem. 2008; 19(12):2440–2445.10.1021/bc800330k [PubMed: 19007261]
79. Yu SS, Scherer RL, Ortega RA, Bell CS, O'Neil CP, Hubbell JA, Giorgio TD. Enzymatic-and temperature-sensitive controlled release of ultrasmall superparamagnetic iron oxides (USPIOs). J Nanobiotech. 2011; 9(1):1–10.10.1186/1477-3155-9-7
80. Westmeyer GG, Durocher Y, Jasanoff A. A secreted enzyme reporter system for MRI. Angew Chemie Int Ed. 2010; 49(23):3909–93911.10.1002/anie.200906712
81. Colomb J, Louie K, Masia SP, Bennett KM. Self-degrading, MRI-detectable hydrogel sensors with macromolecular target sensitivity. Magn Reson Med. 2010; 64:1792–1799.10.1002/mrm.22570 [PubMed: 20648680]
82. Mizukami S, Takikawa R, Sugihara F, Hori Y, Tochio H, Wälchli M, Shirakawa M, Kikuchi K. Paramagnetic relaxation-based ^{19}F MRI probe to detect protease activity. J Am Chem Soc. 2008; 130(3):794–795.10.1021/ja077058z [PubMed: 18154336]
83. Matsushita H, Mizukami S, Mori Y, Sugihara F, Shirakawa M, Yoshioka Y, Kikuchi K. ^{19}F MRI monitoring of gene expression in living cells through cell-surface β-lactamase activity. ChemBioChem. 2012; 13(11):1579–1583.10.1002/cbic.201200331 [PubMed: 22777922]
84. Keliris A, Mamedov I, Hagberg GE, Logothetis NK, Scheffler K, Engelmann J. A smart ^{19}F and ^{1}H MRI probe with self- immolative linker as a versatile tool for detection of enzymes. Contrast Media Molec Imaging. 2012; 7(5):478–483.10.1002/cmmi.1470 [PubMed: 22821882]
85. Yu JX, Kodibagkar VD, Liu L, Mason RP. A ^{19}F-NMR approach using reporter molecule pairs to assess β-galactosidase in human xenograft tumors *in vivo*. NMR Biomed. 2008; 21(7):704–712.10.1002/nbm.1244 [PubMed: 18288788]
86. Li Z, Qiao H, Lebherz C, Choi SR, Zhou X, Gao G, Kung HF, Rader DJ, Wilson JM, Glickson JD, Zhou R. Creatine kinase, a magnetic resonance-detectable marker gene for quantification of liver-directed gene transfer. Hum Gene Ther. 2005; 16(12):1429–1438. [PubMed: 16390274]
87. Chen AP, Hurd RE, Schroeder MA, Lau AZ, Gu Y, Lam WW, Barry J, Tropp J, Cunningham CH. Simultaneous investigation of cardiac pyruvate dehydrogenase flux, Krebs cycle, metabolism and pH, using hyperpolarized [1,2–13C]pyruvate *in vivo*. NMR Biomed. 2012; 25(2):305–311.10.1002/nbm.1749 [PubMed: 21774012]
88. Barb AW, Hekmatyar SK, Glushka JN, Prestegard JH. Probing alanine transaminase catalysis with hyperpolarized ^{13}CD3-pyruvate. J Magn Reson. 2013; 228:59–65.10.1016/j.jmr.2012.12.013 [PubMed: 23357427]
89. Schroeder MA, Ali MA, Hulikova A, Supuran CT, Clarke K, Vaughn-Jones RD, Tyler DJ, Swietach P. Extramitocontrial domain rich in carbonic anhydrase activity improves myocardial energetics. Proc Nat Acad Sci USA. 2013; 110(10):E958–E967.10.1073/pnas.1213471110 [PubMed: 23431149]
90. Lodi A, Woods SM, Ronen SM. Treatment with the MEK inhibitor U0126 induces decreased hyperpolarized pyruvate to lactate conversion in breast, but not prostate, cancer cells. NMR Biomed. 2013; 26(3):299–306.10.1002/nbm.2848 [PubMed: 22945392]
91. Laustsen C, Ostergaard JA, Lauritzen MH, Norregaard R, Bowen S, Sogaard LV, Flybjerg A, Pedersen M, Ardenkjaer-Larsen JH. Assessment of early diabetic renal changes with hyperpolarized [1-^{13}C]pyruvate. Diabetes/Met Res Reviews. 2013; 29(2):125–129.10.1002/dmrr.2370
92. Venkatesh HS, Chaumeil MM, Ward CS, Haas-Kogan DA, David JC, Ronen SM. Reduced phosphocholine and hyperpolarized lactate provide magnetic resonance biomarkers of PI3K/Akt/

mTOR inhibition in glioblastoma. Neuro-Oncol. 2012; 14(3):315–325.10.1093/neuonc/nor209 [PubMed: 22156546]

93. Harrison C, Yang C, Jindal A, DeBerardinis RJ, Hooshyar MA, Merritt M, Sherry AD, Malloy CR. Comparison of kinetic models for analysis of pyruvate-to-lactate exchange by hyperpolarized ^{13}C NMR. NMR Biomed. 2012; 25(11):1286–1294.10.1002/nbm.2801 [PubMed: 22451442]
94. Whitney TH, Kettunen MI, Brindle KM. Kinetic modeling of hyperpolarized ^{13}C label exchange between pyruvate and lactate in tumor cells. J Biol Chem. 2011; 286(28):24572–24580.10.1074/jbc.M111.237727 [PubMed: 21596745]
95. Zierhut ML, Yen YF, Chen AP, Bok R, Albers MJ, Zhang V, Tropp J, Park I, Vigneron DB, Kurhanewicz J, Hurd RE, Nelson SJ. Kinetic modeling of hyperpolarized ^{13}C1-pyruvate metabolism in normal rats and TRAMP mice. J Magn Reson. 2010; 202(1):85–92.10.1016/j.jmr.2009.10.003 [PubMed: 19884027]
96. Gallagher FA, Kettunen MI, Day SE, Lerche M, Brindle KM. ^{13}C MR spectroscopy measurements of glutaminase activity in human hepatocellular carcinoma cells using hyperpolarized ^{13}C-labeled glutamine. Magn Reson Med. 2008; 60(2):253–257.10.1002/mrm.21650 [PubMed: 18666104]
97. Karlsson M, Jensen PR, in't Zandt R, Gisselsson A, Hansson G, Duus JO, Meier S, Lerche MH. Imaging of branched chain amino acid metabolism in tumors with hyperpolarized ^{13}C ketoisocaproate. Int J Cancer. 2010; 127(3):729–736.10.1002/ijc.25072 [PubMed: 19960440]
98. Zacharias NM, Chan HR, Sailasuta N, Ross BD, Bhattacharya P. Real-time molecular imaging of tricarboxylic acid cycle metabolism *in vivo* by hyperpolarized 1-^{13}C diethyl succinate. J Am Chem Soc. 2012; 134(2):934–943.10.1021/ja2040865 [PubMed: 22146049]
99. Keshari KR, Wilson DM, Chen AP, Bok R, Larson PEZ, Hu S, Van Criekinge M, MacDonald JM, Vigneron DB, Kurhanewicz J. Hyperpolarized [2-^{13}C]-fructose: a hemiketal DNP substrate for *in vivo* metabolic imaging. J Am Chem Soc. 2009; 131(48):17591–17596.10.1021/ja9049355 [PubMed: 19860409]
100. Jamin Y, Gabellieri C, Smythe L, Reynolds S, Robinson SP, Springer CJ, Leach MO, Payne GS, Eykyn TR. Hyperpolarized ^{13}C magnetic resonance detection of carboxypeptidase G2 activity. Magn Reson Med. 2009; 62(5):1300–1304.10.1002/mrm.22049 [PubMed: 19780183]
101. Chambers JM, Hill PA, Aaron JA, Han Z, Christianson DW, Kuzma NN, Dmochowski IJ. Cryptophane xenon-129 nuclear magnetic resonance biosensors targeting human carbonic anhydrase. J Am Chem Soc. 2009; 131(2):563–569.10.1021/ja906092w [PubMed: 19140795]
102. Schlundt A, Kilian W, Beyermann M, Sticht J, Gunther S, Hopner S, Falk K, Roetzschke O, Mitschang L, Freund C. A xenon-129 biosensor for monitoring MHC-peptide interactions. Angew Chemie Int Ed. 2009; 48(23):4142–4145.10.1002/anie.200806149
103. Seward GK, Bai Y, Kahn NS, Dmochowski IJ. Cell-compatible, integrin-targeted cryptophane-^{129}Xe NMR biosensors. Chem Science. 2011; 2:1103–1110.10.1039/C1SC00041A
104. Wu Y, Carney CE, Denton M, Hart E, Zhao P, Streblow DN, Sherry AD, Woods M. Polymeric PARACEST MRI contrast agents as potential reporters for gene therapy. Org Biomol Chem. 2010; 8(23):5333–5338.10.1039/c0ob00087f [PubMed: 20848030]
105. Smolensky ED, Peterson KL, Weitz EA, Lewandowski C, Pierre VC. Magnetoluminescent light switches – dual modality in DNA detection. J Am Chem Soc. 2013; 135(24):8966–8972.10.1021/ja402107x [PubMed: 23692333]
106. New K, Andolina CM, Huang CH, Morrow JR. PARACEST properties of a dinuclear neodymium(III) complex bound to DNA or carbonate. Bioconj Chem. 2009; 20(7):1375–1382.10.1021/bc900146z
107. Xu W, Lu Y. A smart magnetic resonance imaging contrast agent responsive to adenosine based on a DNA aptamer-conjugated gadolinium complex. Chem Commun. 2011; 47(17):4998–5000.10.1039/C1CC10161G
108. Roy V, Brotin T, Dutasta JP, Charles MH, Delair T, Mallet F, Huber G, Desvaux H, Boulard Y, Berthault P. A cryptophane biosensor for the detection of specific nucleotide targets through xenon NMR spectroscopy. Chem Phys Chem. 2007; 8(14):2082–2085. [PubMed: 17712828]
109. Lippert AR, Keshari KR, Kurhanewicz J, Chang CJ. A hydrogen peroxide-responsive hyperpolarized ^{13}C MRI contrast agent. J Am Chem Soc. 2011; 133(11):3776–3779.10.1021/ja111589a [PubMed: 21366297]

110. Chan KWY, McMahon MT, Kato Y, Liu G, Bulte JWM, Bhujwalla ZM, Artemov D, van Zijl PC. Natural D-glucose as a biodegradable MRI contrast agent for detecting cancer. Magn Reson Med. 2012; 68(6):1764–1773.10.1002/mrm.24520 [PubMed: 23074027]
111. Walker-Samuel S, Ramasawmy R, Torrealdea F, Rega M, Rajkumar V, Johnson SP, Richardson S, Concalves M, Parkes HG, Arstad E, Thomas DL, Pedley RB, Lythgoe MF, Golay X. *In vivo* imaging of glucose uptake and metabolism in tumors. Nat Med. 2013; 19:1067–1072.10.1038/nm.3252. [PubMed: 23832090]
112. Cai K, Haris M, Singh A, Kogan F, Greenberg JH, Hariharan H, Detre JA, Reddy R. Magnetic resonance imaging of glutamate. Nat Med. 2012; 18(2):302–306.10.1038/nm.2615 [PubMed: 22270722]
113. Haris M, Cai K, Singh A, Hariharan H, Reddy R. In vivo mapping of brain myo-inositol. Neuroimage. 2011; 54(3):2079–2085.10.1016/j.neuroimage.2010.10.017 [PubMed: 20951217]
114. Kogan F, Haris M, Singh A, Cai K, DeBrosse C, Nanga RPR, Hariharan H, Reddy R. Method for high-resolution imaging of creatine in vivo using chemical exchange saturation transfer. Magn Reson Med. 2014; 71(1):164–72.10.1002/mrm.24641 [PubMed: 23412909]
115. Zhang S. Direct detection of hydrogen peroxide via ^{1}H CEST-MRI. Proc Intl Soc Mag Reson Med. 2007; 1:3461.
116. Jordan BF, Magat J, Colliez F, Ozel E, Fruytier AC, Marchand V, Mignion L, Bouzin C, Cani PD, Vandeputte C, Feron O, Delzenne N, Himmelreich U, Denolin V, Duprez T, Gallez B. Mapping of oxygen by imaging lipids relaxation enhancement: A potential sensitive endogenous MRI contrast to map variations in tissue oxygenation. Magn Reson Med. 2013; 70:732–744.10.1002/mrm.24511 [PubMed: 23023932]
117. Kodibagkar VD, Wang X, Pacheco-Torres J, Gulaka P, Mason RP. Proton imaging of siloxanes to map tissue oxygenation levels (PISTOL): a tool for quantitative tissue oximetry. NMR Biomed. 2008; 21:899–907.10.1002/nbm.1279 [PubMed: 18574806]
118. Gulaka PK, Rastogi U, McKay MA, Wang X, Mason RP, Kodibagkar VD. Hexamethyldisiloxane-based nanoprobes for ^{1}H MRI oximetry. NMR Biomed. 2011; 24:1226–1234.10.1002/nbm.1678 [PubMed: 21412864]
119. Battistini E, Mortillaro A, Aime S, Peters JA. Molecular recognition of sugars by lanthanide (III) complexes of a conjugate of N,N-bis[2-[bis[2-(1,1-dimethylethoxy)-2-oxoethyl]amino]ethylglycine and phenylboronic acid. Contrast Media Molec Imaging. 2007; 2(4):163–171.10.1002/cmmi.141 [PubMed: 17640034]
120. Surman AJ, Bonnet CS, Lowe MP, Kenny GD, Bell JD, Toth E, Vilar R. A pyrophosphate-responsive gadolinium(III) MRI contrast agent. Chem Eur J. 2011; 17:223–230.10.1002/chem.201001397 [PubMed: 21207619]
121. Shapiro MG, Westmeyer GG, Romero PA, Szablowski JO, Kuster B, Shah A, Otey C, Langer R, Arnold FH, Jasanoff A. Directed evolution of a magnetic resonance imaging contrast agent for noninvasive imaging of dopamine. Nat Biotechnol. 2010; 28(3):264–270.10.1038/nbt.1609 [PubMed: 20190737]
122. Brustad EM, Lelyveld VS, Snow C, Crook N, Jung ST, Martinez FM, Scholl TJ, Jasanoff A, Arnold FH. Structure-guided directed evolution of highly selective P450-based magnetic resonance imaging sensors for dopamine and serotonin. J Mol Biol. 2012; 422(2):245–262.10.1016/j.jmb.2012.05.029 [PubMed: 22659321]
123. Huang CH, Morrow JR. A PARACEST agent responsive to inner- and outer-sphere phosphate ester interactions for MRI applications. J Am Chem Soc. 2009; 131(12):4206–4207.10.1021/ja900290z [PubMed: 19317496]
124. Calabrese V, Guagliano E, Sapienza M, Mancuso C, Butterfield DA, Giuffrida SAM. Redox regulation of cellular stress response in neurodegenerative disorders. Ital J Biochem. 2006; 55(3–4):263–282. [PubMed: 17274531]
125. Tochhawng L, Deng S, Pervaiz S, Yap CT. Redox regulation of cancer cell migration and invasion. Mitochondrion. 2013; 13(3):246–253.10.1016/j.mito.2012.08.002 [PubMed: 22960576]
126. Zhelev Z, Gadjeva V, Aoki I, Bakalova R, Saga T. Cell-penetrating nitroxides as molecular sensors for imaging of cancer *in vivo*, based on tissue redox activity. Mol Biosyst. 2012; 8(10):2733–2740.10.1039/c2mb25128k [PubMed: 22832934]

127. Loving GS, Mukherjee S, Caravan P. Redox-activated manganese-based MR contrast agent. J Am Chem Soc. 2013; 135(12):4620–4623.10.1021/ja312610j [PubMed: 23510406]
128. Tsitovich PV, Spernyak JA, Morrow JR. A redox-activated MRI contrast agent that switches between paramagnetic and diamagnetic states. Angew Chem Int Ed. 2013; 52:13997–14000.10.1002/anie.201306394
129. Keshari KR, Kurhanewicz J, Bok R, Larson PEZ, Vigneron DB, Wilson DM. Hyperpolarized ^{13}C dehydrascorbate as an endogenous redox sensor for *in vivo* metabolic imaging. Proc Nat Acad Sci USA. 2011; 108(46):18606–18611.10.1073/pnas.1106920108 [PubMed: 22042839]
130. Liu VH, Vassiliou CC, Imaad SM, Cima MJ. Solid MRI contrast agents for long-term, quantitative in vivo oxygen sensing. Proc Nat Acad Sci USA. 2014; 111:6588–6593.10.1073/pnas.1400015111 [PubMed: 24753603]
131. Ratnakar SJ, Viswanathan S, Kovacs Z, Jindal AK, Green KN, Sherry AD. Europium(III) DOTA-tetraamide complexes as redox-active MRI sensors. J Am Chem Soc. 2012; 134(13):5798–5800.10.1021/ja211601k [PubMed: 22420507]
132. Song B, Wu Y, Yu M, Zhao P, Zhou C, Kiefer GE, Sherry AD. A europium(III)-based PARACEST agent for sensing singlet oxygen by MRI. Dalton Trans. 2013; 42:8066–8069.10.1039/c3dt50194a [PubMed: 23575743]
133. Yu M, Beyers RJ, Gorden JD, Cross JN, Goldsmith CR. A magnetic resonance imaging contrast agent capable of detecting hydrogen peroxide. Inorg Chem. 2012; 51(17):9153–9155.10.1021/lic3012603 [PubMed: 22889331]
134. Tu C, Osborne EA, Louie AY. Synthesis and characterization of a redox- and light-sensitive MRI contrast agent. Tetrahedron. 2009; 65(7):1241–1246.10.1016/j.tet.2008.12.020 [PubMed: 20126289]
135. Iwaki S, Hanaoka K, Piao W, Komatsu T, Ueno T, Terai T, Nagano T. Development of hypoxia-sensitive Gd^{3+}-based MRI contrast agents. Bioorg Med Chem Lett. 2012; 22(8):2798–2802.10.1016/j.bmcl.2012.02.071 [PubMed: 22424977]
136. Winter MB, Klemm PJ, Phillips-Piro CM, Raymond KN, Marletta MA. Porphyrin-substituted H-NOX proteins as high-relaxivity MRI contrast agents. Inorg Chem. 2013; 52:2277–2279.10.1021/ic302685h [PubMed: 23394479]
137. Raghunand N, Jagadish B, Trouard TP, Galons JP, Gillies RJ, Mash EA. Redox-sensitive contrast agents for MRI based on reversible binding of thiols to serum albumin. Magn Reson Med. 2006; 55(6):1272–1280.10.1002/mrm.20904 [PubMed: 16700014]
138. Hille, B. Ion Channels of Excitable Membranes. 3. Sinauer; Sunderland, MA: 2001.
139. Sayre LM, Perry G, Atwood CS, Smith MA. The role of metals in neurodegenerative diseases. Cell Mol Biol. 2000; 46:731–741. [PubMed: 10875436]
140. Haraguchi H. Metallomics as integrated biometal science. J Analyt Atomic Spect. 2004; 19:5–14.
141. Que EL, Chang CJ. A smart magnetic resonance contrast agent for selective copper sensing. J Am Chem Soc. 2006; 128(50):15942–15943.10.1021/ja065264l [PubMed: 17165700]
142. Major JL, Parigi G, Luchinat C, Meade TJ. The synthesis and *in vitro* testing of a zinc-activated MRI contrast agent. Proc Nat Acad Sci USA. 2007; 104(35):13881–13886. [PubMed: 17724345]
143. Dhingra K, Maier ME, Beyerlein M, Angelovski G, Logothetis NK. Synthesis and characterization of a smart contrast agent sensitive to calcium. Chem Comm. 2008; 7(29):3444–3446.10.1039/b801975d [PubMed: 18633517]
144. Dhingra K, Fouskova P, Angelovski G, Maier ME, Logothetis NK, Toth E. Towards extracellular Ca^{2+} sensing by MRI: Synthesis and calcium-dependent ^{1}H and ^{17}O relaxation studies of two novel bismacrocyclic Gd^{3+} complexes. J Biol Inorg Chem. 2008; 13(1):35–46.10.1007/s00775-007-0296-9 [PubMed: 17874148]
145. Que EL, Gianolio E, Baker SL, Wong AP, Aime S, Chang CJ. Copper-responsive magnetic resonance imaging contrast agents. J Am Chem Soc. 2009; 131(24):8527–8536.10.1021/ja900884j [PubMed: 19489557]
146. Jang JH, Bhuniya S, Kang J, Yeom A, Hong KS, Kim JS. Cu^{2+}-responsive bimodal (optical/MRI) contrast agent for cellular imaging. Org Lett. 2013; 15:4702–4705.10.1021/ol4025293 [PubMed: 24015763]

147. Esqueda AC, López JA, Andreu-de-Riquer G, Alvarado-Monzón JC, Ratnakar J, Lubag AJM, Sherry AD, De León-Rodríguez LM. A new gadolinium-based MRI zinc sensor. J Am Chem Soc. 2009; 131(32):11387–11391.10.1021/ja901875v [PubMed: 19630391]

148. Lubag AJ, De León-Rodríguez LM, Burgess SC, Sherry AD. Noninvasive MRI of β-cell function using a Zn^{2+}-responsive contrast agent. Proc Nat Acad Sci USA. 2011; 108(45):18400–18405.10.1073/pnas.1109649108 [PubMed: 22025712]

149. Zhang X, Lovejoy KS, Jasanoff A, Lippard SJ. Water-soluble porphyrins as a dual-function molecular imaging platform for MRI and fluorescence zinc sensing. Proc Nat Acad Sci USA. 2008; 104(26):10780–10785.10.1073/pnas.0702393104 [PubMed: 17578918]

150. Trokowski R, Ren J, Kálmán FK, Sherry AD. Selective sensing of zinc ions with a PARACEST contrast agent. Angew Chem Int Ed. 2005; 44(42):6920–6923.10.1002/anie.200502173

151. Paris J, Gameiro C, Humblet V, Mohapatra PK, Jaques V, Desreux JF. Auto-assembling of ditopic macrocyclic lanthanide chelates with transition-metal ions. Rigid multimetallic high relaxivity contrast agents for magnetic resonance imaging. Inorg Chem. 2006; 45(13):5092–5102.10.1021/ic0603050 [PubMed: 16780331]

152. Parac-Vogt TN, Vander Elst L, Kimpe K, Laurent S, Burtea C, Chem F, Van Deun R, Ni Y, Muller RN, Binnemans K. Pharmacokinetic and in vivo evaluation of a self-assembled gadolinium(III)-iron(II) contrast agent with high relaxivity. Contrast Media Molec Imaging. 2006; 1(6):267–278.10.1002/cmmi.114 [PubMed: 17191767]

153. Kubíček V, Vitha T, Kotek J, Hermann P, Vander Elst L, Muller RN, Lukes I, Peters JA. Towards MRI contrast agents responsive to Ca(II) and Mg(II) ions: metal-induced oligomerization of dota-bisphosphonate conjugates. Contrast Media Molec Imaging. 2010; 5(5):294–296.10.1002/cmmi.386 [PubMed: 20973114]

154. Xu W, Xing H, Lu Y. A smart T1-weighted MRI contrast agent for uranyl cations based on a DNAzyme-gadolinium conjugate. Analyst. 2013; 138:6266–6269.10.1039/C3AN01182H [PubMed: 24005082]

155. Kotera N, Tassali N, Leonce E, Boutin C, Berthault P, Brotin T, Dutasta JP, Delacour L, Traore T, Buisson DA, Taran F, Coudert S, Rousseau B. A sensitive zinc-activated ^{129}Xe MRI probe. Angew Chemie Int Ed. 2012; 51(17):4100–4103.10.1002/anie.201109194

156. Kitamura M, Suzuki T, Abe R, Ueno T, Aoki S. ^{11}B NMR sensing of d-block metal ions *in vitro* and in cells based on the carbon–boron bond cleavage of phenylboronic acid-pendant cyclen (Cyclen = 1,4,7,10-Tetraazacyclododecane). Inorg Chem. 2011; 50(22):11568–11580.10.1021/ic201507q [PubMed: 22010826]

157. Angelovski G, Chauvin T, Pohmann R, Logothetis NK, Toth E. Calcium-responsive paramagnetic CEST agents. Bioorg Med Chem. 2011; 19:1097–1105.10.1016/j.bmc.2010.07.023 [PubMed: 20691598]

158. Warburg, O. The metabolism of tumours. Constable; London, UK: 1930.

159. Raghunand N, Gillies RJ. pH and chemotherapy. Novartis Found Symp. 2001; 240:199–211. [PubMed: 11727930]

160. Robey IF, Baggett BK, Kirkpatrick ND, Roe DJ, Dosescu J, Sloane BF, Hashim AI, Morse DL, Raghunand N, Gatenby RA, Gillies RA. Bicarbonate increases tumor pH and inhibits spontaneous metastases. Cancer Res. 2009; 69(6):2260–2268.10.1158/0008-5472.CAN-07-5575 [PubMed: 19276390]

161. Manchun S, Dass CR, Sriamornsak P. Targeted therapy for cancer using pH-responsive nanocarrier systems. Life Sci. 2012; 90(11–12):381–387.10.1016/j.lfs.2012.01.008 [PubMed: 22326503]

162. Kim T, Cho E, Chae Y, Kim M, Oh A, Jin J. Urchin-shaped manganese oxide nanoparticles as pH-responsive activatable T1 contrast agents for magnetic resonance imaging. Angew Chemie Int Ed. 2011; 50(45):10589–10593.10.1002/anie.20113108

163. Chen Y, Yin Q, Ji X, Zhang S, Chen H, Zheng Y, Sun Y, Qu H, Wang Z, Li Y, Wang X, Zhang K, Zhang L, Shi J. Manganese oxide-based multifunctionalized mesoporous silica nanoparticles for pH-responsive MRI, ultrasonography and circumvention of MDR in cancer cells. Biomaterials. 2012; 33(29):7126–7137.10.1016/j.biomaterials.2012.06.059 [PubMed: 22789722]

164. Torres E, Mainini F, Napolitano R, Fedeli F, Cavalli R, Aime S, Terreno E. Improved paramagnetic liposomes for MRI visualization of pH triggered release. J Control Rel. 2011; 154(2):196–202.10.1016/j.jconrel.2011.05.017

165. Kim KS, Park W, Hu J, Bae YH, Na K. A cancer-recognizable MRI contrast agents using pH-responsive polymeric micelle. Biomaterials. 2014; 35:337–343.10.1016/j.biomaterials.2013.10.004 [PubMed: 24139764]

166. Lin CW, Tseng SJ, Kempson IM, Yang SC, Hong TM, Yang PC. Extracellular delivery of modified oligonucleotide and superparamagnetic iron oxide nanoparticles from a degradable hydrogel triggered by tumor acidosis. Biomaterials. 2013; 34(17):4387–4393.10.1016/j.biomaterials.2013.02.058 [PubMed: 23478033]

167. Gao GH, Im GH, Kim MS, Lee JW, Yang J, Jeon H, Lee JH, Lee DS. Magnetite-nanoparticle-encapsulated pH-responsive polymeric micelle as an MRI probe for detecting acidic pathologic areas. Small. 2010; 6(11):1201–1204.10.1002/smll.200902317 [PubMed: 20449849]

168. Okada S, Mizukami S, Kikuchi K. Switchable MRI contrast agents based on morphological changes of pH-responsive polymers. Bioorg Med Chem. 2012; 20(2):760–774.10.1016/j.bmc.2011.12.005

169. Giovenzana GB, Negri R, Rolla GA, Tei L. Gd-aminoethyl-DO3A complexes: a novel class of pH-sensitive MRI contrast agents. Euro J Inorg Chem. 2012; 12:2035–2039.10.1002/ejic.201101296

170. Werner EJ, Botta M, Aime S, Raymond KN. Effect of a mesitylene-based ligand cap on the relaxometric properties of Gd(III) hydroxypyridonate MRI contrast agents. Contrast Media Molec Imaging. 2009; 4(5):220–229.10.1002/cmmi.281 [PubMed: 19839031]

171. Wu Y, Soesbe TC, Kiefer GE, Zhao P, Sherry AD. A responsive europium(III) chelate that provides a direct readout of pH by MRI. J Am Chem Soc. 2010; 132:14002–14003.10.1021/ja106018n [PubMed: 20853833]

172. Delli Castelli D, Terreno E, Aime S. Yb(III)-HPDO3A: a dual pH-and temperature-responsive CEST agent. Angew Chem Int Ed. 2011; 50(8):1798–1800.10.1002/anie.201007105

173. Sheth VR, Li Y, Chen LQ, Howison CM, Flask CA, Pagel MD. Measuring *in vivo* tumor pH with CEST-FISP MRI. Magn Reson Med. 2012; 67(3):760–768.10.1002/mrm.23038 [PubMed: 22028287]

174. Liu G, Li Y, Sheth VR, Pagel MD. Imaging in vivo extracellular pH with a single paramagnetic chemical exchange saturation transfer magnetic resonance imaging contrast agent. Molec Imaging. 2012; 11(1):47–57. [PubMed: 22418027]

175. McVicar N, Li AX, Suchy M, Hudson RHE, Menon RS, Bartha R. Simultaneous *in vivo* pH and temperature mapping using a PARACEST-MRI contrast agent. Magn Reson Med. 2013; 70(4):1016–1025.10.1002/mrm.24539 [PubMed: 23165779]

176. Dorazio SJ, Olatune AO, Spernyak JA, Morrow JA. CoCEST: cobalt(II) amide-appended paraCEST MRI contrast agents. ChemComm. 2013; 49:10025–10027.10.1039/c3cc45000g

177. Chen LQ, Howison CM, Jeffery JJ, Robey IF, Kuo PH, Pagel MD. Evaluations of extracellular pH within in vivo tumors using acidoCEST MRI. Magn Reson Med. 201310.1002/mrm.25053

178. Longo DL, Dastru W, Digilio G, Keupp J, Langereis S, Lanzardo S, Prestigio S, Steinbach O, Terreno E, Uggeri F, Aime S. Iopamidol as a responsive MRI-chemical exchange saturation transfer contrast agent for pH mapping of kidneys: *In vivo* studies in mice at 7T. Magn Reson Med. 2011; 65(1):202–211.10.1002/mrm.22608 [PubMed: 20949634]

179. Palussière J, Salomir R, Le Bail B, Fawaz R, Quesson B, Grenier N, Moonen CT. Feasibility of MR-guided focused ultrasound with real-time temperature mapping and continuous sonication for ablation of VX2 carcinoma in rabbit thigh. Magn Reson Med. 2003; 49(1):89–98.10.1002/mrm.10328 [PubMed: 12509823]

180. Shao P, Wang B, Wang Y, Li J, Zhang Y. The application of thermosensitive nanocarriers in controlled drug delivery. J Nanomat. 2011; 38964010.1155/2011/389640

181. de Senneville BD, Quesson B, Moonen CTW. Magnetic resonance temperature mapping. Int J Hyperthermia. 2005; 21(6):515–531. [PubMed: 16147437]

182. de Smet M, Langereis S, van den Bosch S, Grüll H. Temperature-sensitive liposomes for doxorubicin delivery under MRI guidance. J Control Rel. 2010; 143(1):120–127.10.1016/j.jconrel.2009.12.002

183. Settecase F, Sussman MS, Roberts TPL. A new temperature-sensitive contrast mechanism for MRI: Curie temperature transition-based imaging. Contrast Media Molec Imaging. 2007; 2(1): 50–54.10.1002/cmmi.120 [PubMed: 17304641]

184. Zhang S, Malloy CR, Sherry AD. MRI thermometry based on PARACEST agents. J Am Chem Soc. 2005; 127(50):17572–17573.10.1021/ja053799t [PubMed: 16351064]

185. Li AX, Wojciechowski F, Suchy M, Jones CK, Hudson RHE, Menon RS, Bartha R. A sensitive PARACEST contrast agent for temperature MRI: Eu^{3+}-DOTAM-glycine(Gly)-phenylalanine(Phe). Magn Reson Med. 2008; 59(2):374–381.10.1002/mrm.21482 [PubMed: 18228602]

186. Stevens TK, Milne M, Elmehriki AAH, Suchy M, Bartha R, Hudson RHE. A DOTAM-based paraCEST agent favoring TSAP geometry for enhanced amide proton chemical shift dispersion and temperature sensitivity. Contrast Media Molec Imaging. 2013; 8:289–292.10.1002/cmmi.1527 [PubMed: 23606433]

187. Giepmans BNG, Adams SR, Ellisman MH, Tsien RY. The fluorescent toolbox for assessing protein location and function. Science. 2006; 312(5771):217–224.10.1126/science.1124618 [PubMed: 16614209]

188. Prescher JA, Contag CH. Guided by the light: visualizing biomolecular processes in living animals with bioluminescence. Current Opin Chem Biol. 2010; 14(1):80–89.10.1016/j.cbpa.2009.11.001

189. Mitchell GS, Gill RK, Boucher DL, Li C, Cherry SR. *In vivo* Cerenkov luminescence imaging: a new tool for molecular imaging. Phil Trans Royal Soc A: Math Phys Eng Sci. 2011; 369(1955): 4605–4619.10.1098/rsta.2011.0271

190. Osborne EA, Jarrett BR, Tu C, Louie AY. Modulation of T2 relaxation time by light-induced, reversible aggregation of magnetic nanoparticles. J Am Chem Soc. 2010; 132(17):5934–5935.10.1021/ja100254m [PubMed: 20373802]

191. Shan L, Chopra A, Leung K, Eckelman WC, Menkens AE. Characterization of nanoparticle-based contrast agents for molecular magnetic resonance imaging. J Nanopart Res. 2012; 13:1122–1133.

192. Vaughan JT, Snyder CJ, DelaBarre LJ, Bolan PJ, Tian J, Bolinger L, Adriany G, Andersen P, Strupp J, Ugurbil K. Whole-body imaging at 7T: Preliminary results. Magn Reson Med. 2009; 61:244–248.10.1002/mrm.21751 [PubMed: 19097214]

193. Pagel, MD.; Basilion, JP. Non-invasive imaging of genes and gene expression with magnetic resonance imaging and magnetic resonance spectroscopy. In: Gambhir, SS.; Yaghoubi, SS., editors. Molecular Imaging with Reporter Genes. Cambridge University Press; 2011.

194. Auricchio A, Zhou R, Wilson JM, Glickson JD. In vivo detection of gene expression in liver by ^{31}P nuclear magnetic resonance spectroscopy employing creatine kinase as a marker gene. Proc Natl Acad Sci USA. 2001; 98:5205–5210. [PubMed: 11296261]

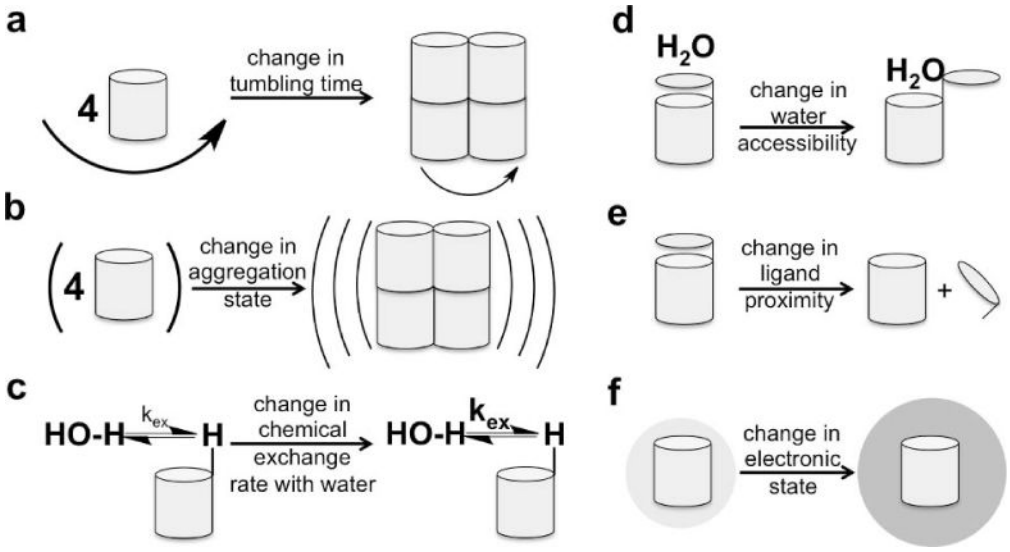

Figure 1.

Schematic of the six physicochemical mechanisms that can be exploited to create a responsive MRI contrast agent: a) a change in tumbling time; b) a change in aggregation state that changes superparamagnetism; c) a change in chemical exchange rate between the agent and water; d) a change in water accessibility; e) a change in ligand proximity; f) a change in electronic state.

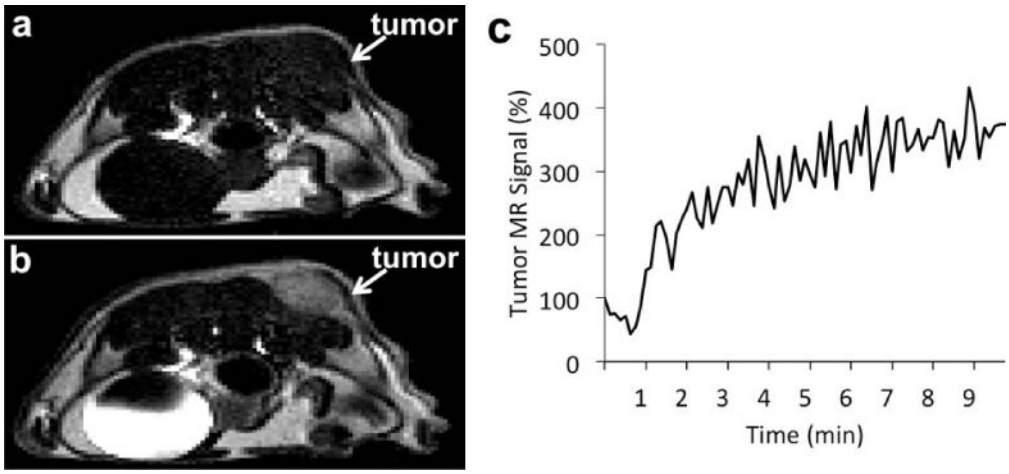

Figure 2.

Monitoring a T_1 MRI contrast agent within *in vivo* tissues. a) An axial MR image of a xenograft tumor model of MDA-MB-231 mammary carcinoma before injection, and b) after injection of 0.1 mmol/kg of Gd-DTPA (Magnevist™) showed a brighter image in the tumor due to accumulation of the agent. c) The temporal change in T_1-weighted MR signal of the tumor can be used to track the dynamic uptake of the agent in the tumor. (Pagel, unpublished results).

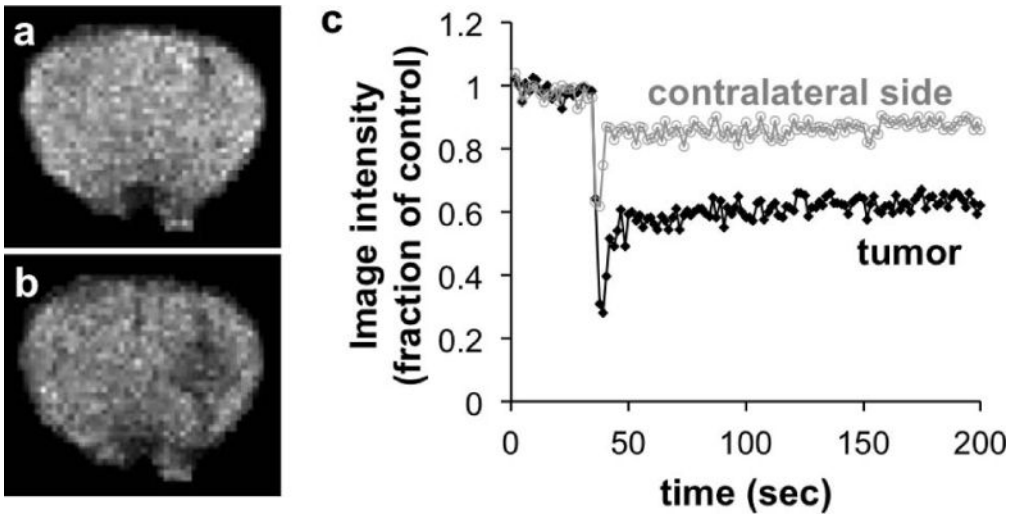

Figure 3.

Monitoring a T_2* MRI contrast agent within *in vivo* tissues. a) A brain MR image (with nonbrain areas masked) of an intracerebral mouse tumor model before injection, and b) after injection of 26.9 μg Fe/g of Feridex® showed a darker image in the tumor due to accumulation of the agent. c) The temporal change in T_2*-weighted MR signal was used to track the enhanced uptake of the agent in the tumor, relative to lower uptake in the contralateral side of the brain. Reproduced with permission from (30).

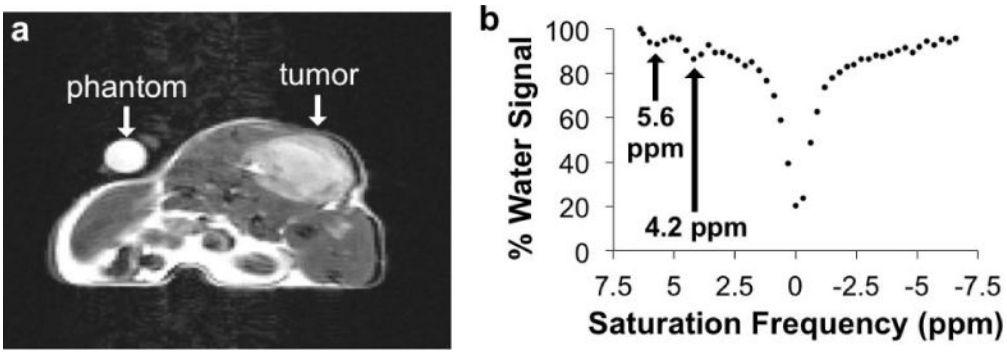

Figure 4.

Monitoring a CEST MRI contrast agent within *in vivo* tissues. a) An axial MR image of a xenograft tumor model of MDA-MB-231 mammary carcinoma before injection showed the location of the tumor. b) The MR signals from the tumor region were measured in images acquired with a series of selective saturation frequencies, which were used to create a CEST spectrum. The CEST effects at 5.6 and 4.2 ppm arose from the exchangeable amide protons of the CEST agent, and the decreased water signal shown at 0 ppm arose from direct saturation of water. (Chen, Howison and Pagel, unpublished results).

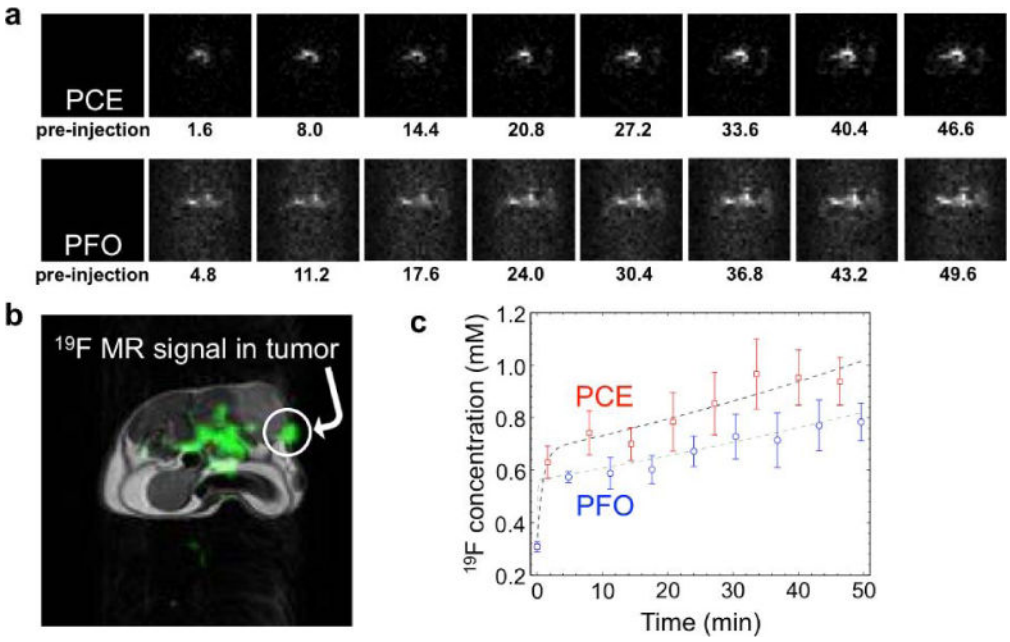

Figure. 5.

Monitoring two ^{19}F nanoemulsions during an *in vivo* MRI study. a) The ^{19}F MRI results of a mouse model with a MDA-MB-231 tumor after co-injection of perfluorocrownether (PCE) and perfluorooctane (PFO) showed accumulation of each agent in the tumor tissue. The time point in units of minutes is listed below each image. b) A ^{1}H MR image (grayscale) provides an anatomical reference for the ^{19}F MRI signal (green), which demonstrates that a region of the tumor showed substantial ^{19}F MR signal. C) The ^{19}F concentrations of PCE and PFO show a similar temporal dependence in tumor tissue. Reproduced with permission from (37).

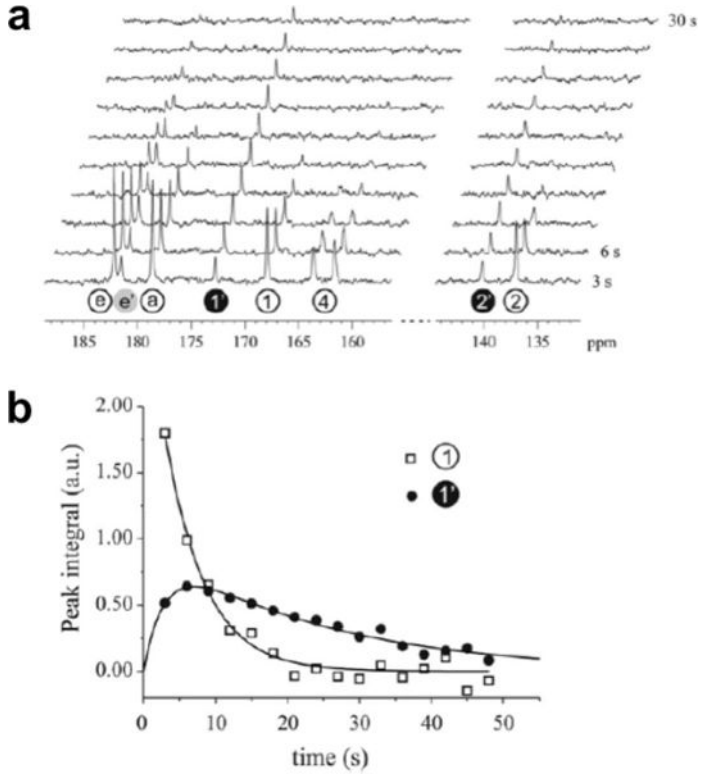

Fig. 6.

Montoring a hyperpolarized ^{13}C MRS agent during an *in vivo* MR study. A) Serial ^{13}C MR spectra recorded every 3 seconds following addition of hyperpolarized 3,5-DFBGlu to 10 units of carboxypeptidase G2 were used to generate b) integrals of the parent peak 1 and its metabolic product 1′, which showed dynamic changes due to carboxypeptidase G2 activity. Reproduced with permission from (100).

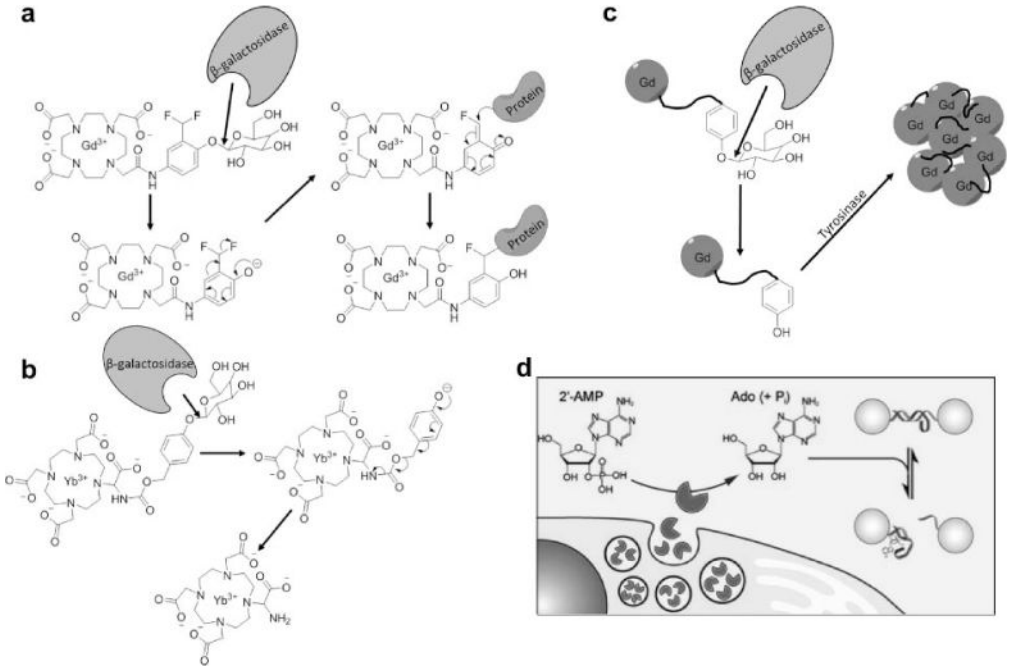

Figure 7.

Responsive MRI contrast agents can detect enzyme activities using a multistep approach. a) β-galactosidase hydrolyzes a β-galactopyranose ligand, forming a reactive phenolate anion that binds the contrast agent to a protein, slowing the tumbling time of the contrast agent and decreasing T_1 relaxation time constant (59). b) β-galactosidase hydrolyzes the same ligand on CEST agent, forming an electron donating group that promotes aromatic delocalization that creates an amine group that can generate CEST (55). c) β-galactosidase-catalyzed hydrolysis of the same ligand creates a tyrosine ligand that can be polymerized by tyrosinase, creating a large molecular system with a slower tumbling time with decreased T_1 relaxation time constant (62). d) Secreted alkaline phosphatase de-phosphorylates 2′-AMP to create adenosine, which can disrupt a DNA duplex that links SPIONs, which increases T_2* relaxation time constant. Figure 7d was reproduced with permission from (80).

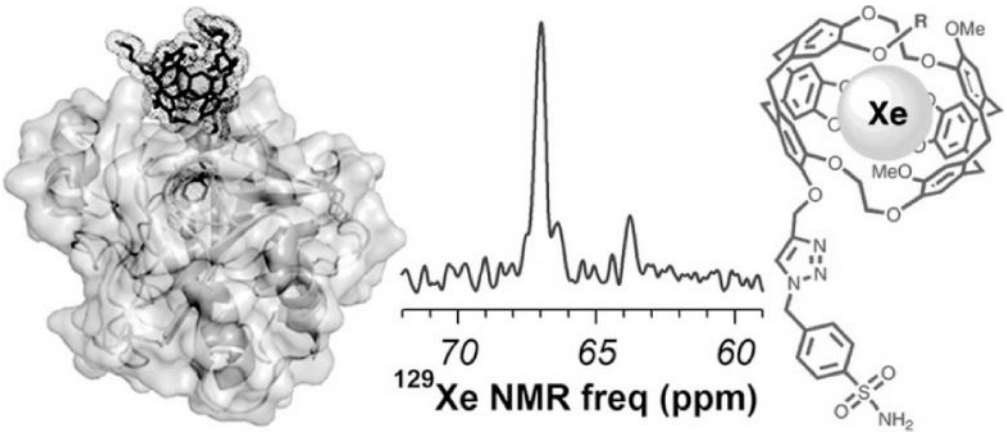

Figure 8.

Protein detection with hyperpolarized ^{129}Xe MRS. A xenon-binding cryptophane with a *p*-benzenesulfonamide ligand (right) can noncovalently bind to carbonic anhydrase IX (left). The binding causes a 3.2 ppm shift in the ^{129}Xe MR spectrum, from 63.7 ppm for the unbound agent to 66.9 ppm for the bound agent (center). Reproduced with permission from reference (101).

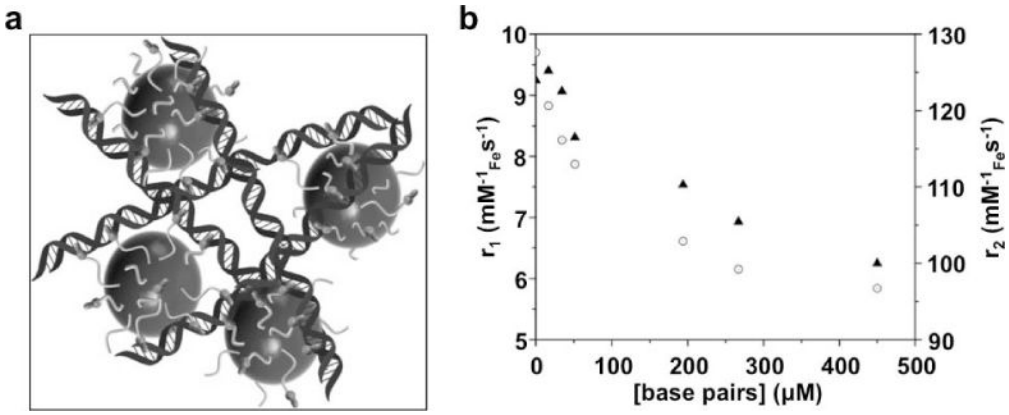

Figure 9.

Nucleic acid detection with a T_2* MRI contrast agent. A) Intercalation of the agent's ligands into the DNA double helix causes aggregation of the iron oxide nanoparticles. b) The aggregation decreases r_2 relaxivity (circles) that indicates an increase in the T_2* relaxation time constant. The r_1 relaxivity (triangles) also decreased following aggregation. Reproduced with permission from reference (105).

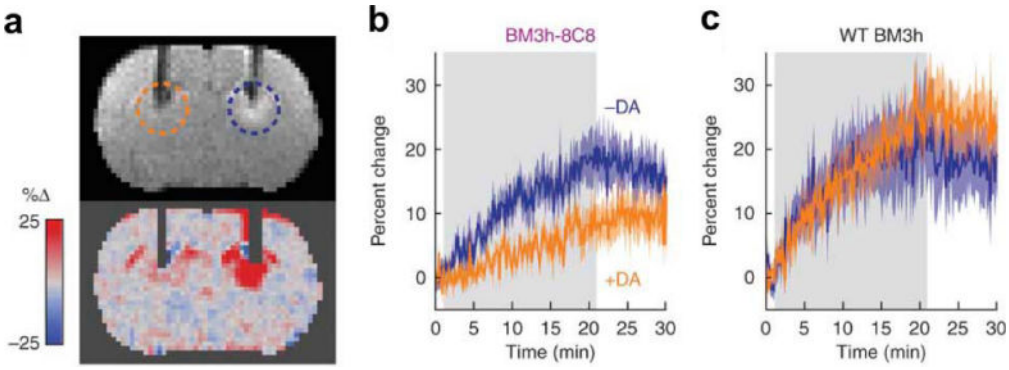

Figure 10.

Detecting a metabolite with a responsive MRI contrast agent. The BM3h-8C8 agent was developed through directed evolution to bind dopamine to the protein's heme group. a) A coronal MR image from a rat injected with BM3h-8C8 in the presence (orange dashed circle) or absence (blue dashed circle) of equimolar dopamine. MRI hyperintensity is noticeable near the tip of the dopamine-free cannula, indicating a short T_1 relaxation time constant, while the lack of hyperintensity at the dopamine cannula indicates a long T_1 relaxation time constant for the system in the presence of this agent. b,c) The temporal change in T_1-weighted MRI signal shows a relative decrease in T_1-weighting in the presence of dopamine (orange) in the rat treated with BM3h-8C8 relative to the rat treated with the wildtype BM3h protein that does not bind to dopamine. Reproduced with permission from reference (121).

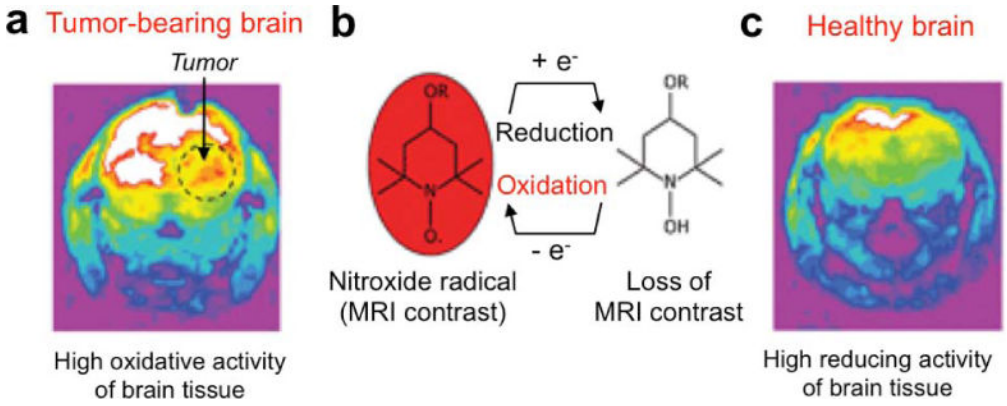

Figure 11.

Detection of *in vivo* redox state with a responsive MRI contrast agent. T_1-weighted MR images were acquired 2 minutes after injection of the nitroxide. a) Reduction of the nitroxide in the tumor tissue caused a loss of MR contrast due to a longer T_1 relaxation time constant. b) The reduction of the nitroxide causes a loss of the radical form. c) The same study was performed with a healthy brain, which showed highly reducing activity that caused a loss of MR contrast from the agent in the brain. Reproduced with permission from reference (126).

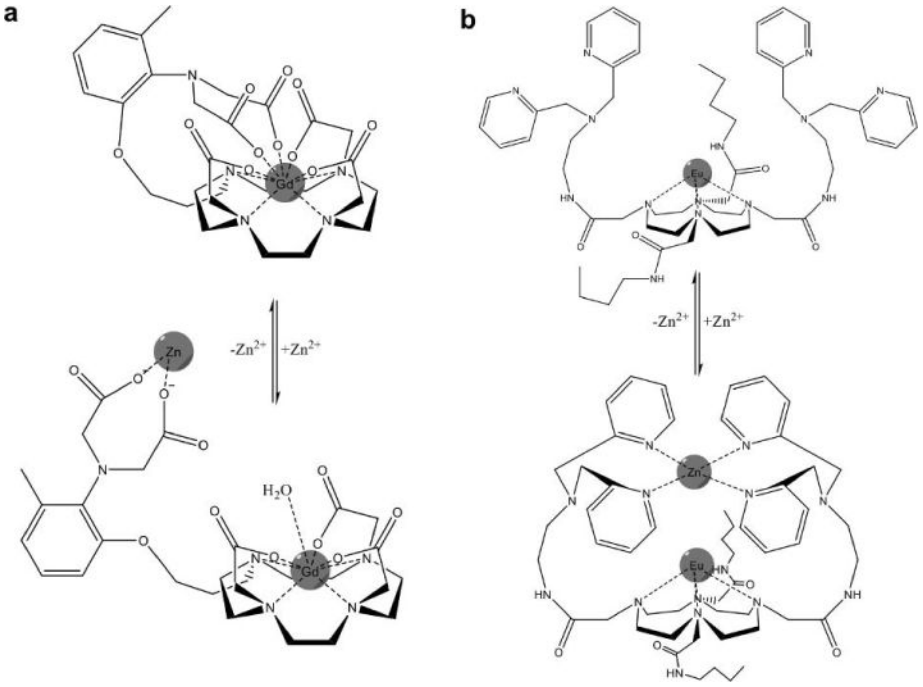

Figure 12.

Responsive MRI contrast agents that detect zinc. a) The ligand of a Gd(III) chelate changes conformation when the ligand binds to Zn^{2+}, which improves water access to Gd(III) and decreases T_1 relaxation time constant (142). b) Two ligands of a Eu(III) chelate change conformation when the ligands bind to Zn^{2+}, which accelerates the chemical exchange of water coordinated to the Eu(III) and improves CEST (150).

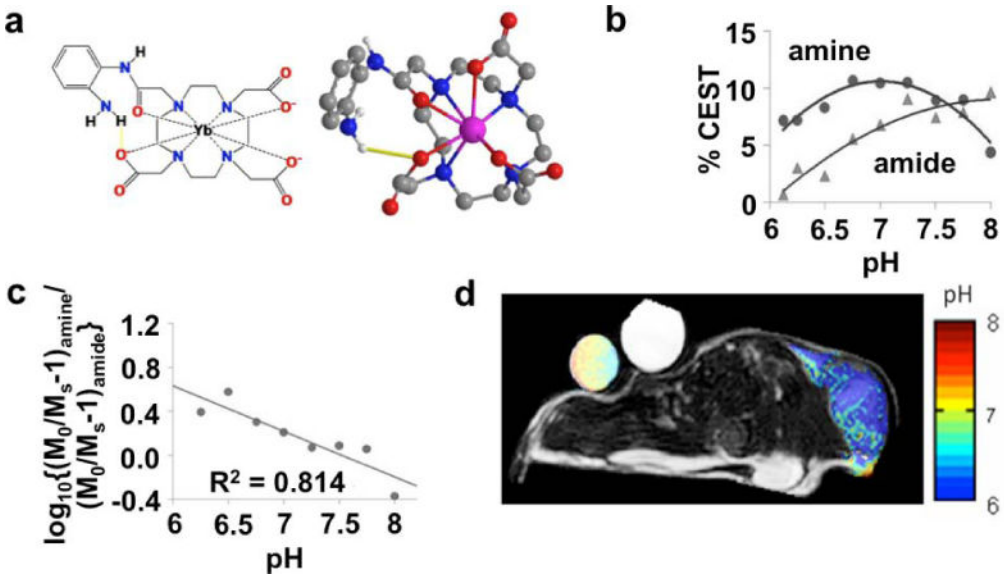

Figure 13.

A MRI contrast agent that measures extracellular pH within *in vivo* tumor tissue. a) 2-dimensional and 3-dimensional models of Yb-DO3A-oAA shows that the proximity of Yb(III) to the amide and the amine causes a shift in the magnetic resonance frequencies of these labile protons, which facilitates CEST MRI studies. b) The CEST effects from the amide and amine are dependent on pH. c) A $\log_{10}$ ratio of the CEST effects is linearly related to pH. d) A parametric pH map of a mouse tumor model overlaid on an anatomic MR image shows an acidic extracellular environment in the tumor region. The agent was directly injected into the tumor tissue to generate strong CEST signals in the tumor. Significant CEST signals were not detected elsewhere in the mouse model. Reproduced with permission from (174).

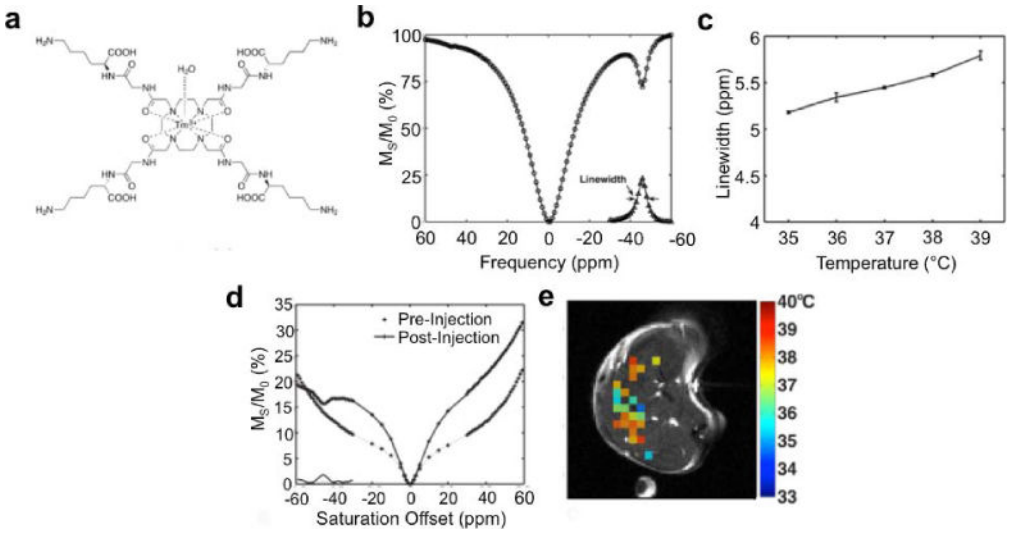

Figure 14.

Temperature measurement with CEST MRI. A) The chemical structure of Tm-DOTA-Gly-Lys shows amide protons that are proximal to the Tm(III) metal. B) This proximity causes a highly shifted CEST effect at −50 ppm. C) The linewidth of this CEST effect is correlated with temperature. D) The linewidth of the CEST peak in an *in vivo* CEST spectrum e) can be used to generate a parametric map of *in vivo* temperature. Reproduced with permission from reference (175).

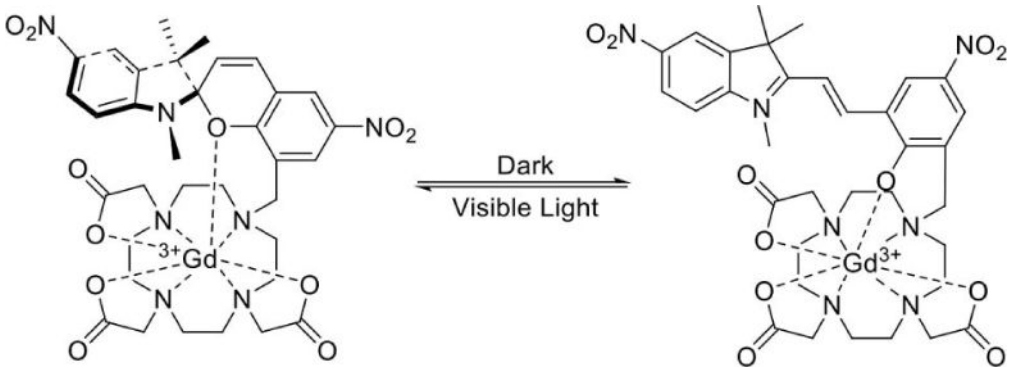

Figure 15.

A unique light-responsive MRI contrast agent with a merocyanine motif (right) can be converted to a spiropyran motif (left) with light at 563 nm wavelength, which increases the T_1 relaxation time constant (134).

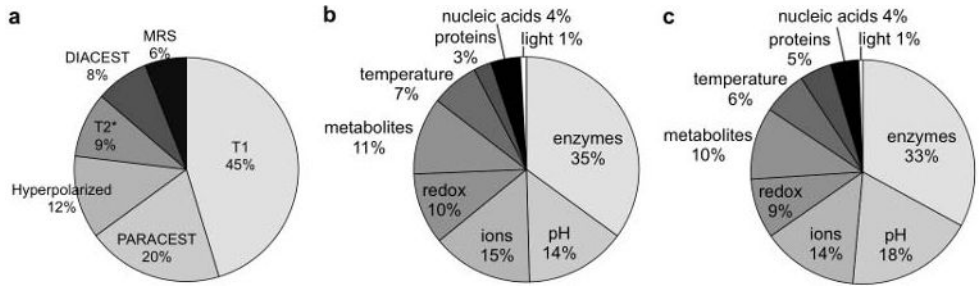

Figure 16.

The distributions of responsive MRI contrast agents. 117 responsive MRI contrast agents were reported in 2005–2014, and have been categorized with regard to a) detection mechanism and b) biomarker. c) The distribution of 171 responsive MRI contrast agents reported in this current review and our previous review (17) is also shown.